THE HIGH-^{240}Pu SECTOR EXPERIMENTS IN ZPPR ASSEMBLY 4

by

H. F. McFarlane and C. L. Beck

The facilities of Argonne National Laboratory are owned by the United States Government. Under the terms of a contract (W-31-109-Eng-38) between the U. S. Energy Research and Development Administration, Argonne Universities Association and The University of Chicago, the University employs the staff and operates the Laboratory in accordance with policies and programs formulated, approved and reviewed by the Association.

ANL-76-112

ARGONNE NATIONAL LABORATORY
9700 South Cass Avenue
Argonne, Illinois 60439

THE HIGH-^{240}Pu SECTOR EXPERIMENTS
IN ZPPR ASSEMBLY 4

by

H. F. McFarlane and C. L. Beck

Applied Physics Division

December 1976

TABLE OF CONTENTS

LIST OF TABLES

LIST OF TABLES (cont.)

LIST OF FIGURES

The High-^{240}Pu Sector Experiment in ZPPR Assembly 4

by

H.F. McFarlane and C.L. Beck

ABSTRACT

The complete high-^{240}Pu fuel experiment in ZPPR assembly 4
is reviewed. Results of criticality, enrichment, small-sample
perturbation, sodium void, ^{238}U Doppler, control rod substitu-
tion and reaction rate measurements are presented. Comparison
of these measured values with calculated results are included
where possible. The relationship between the ZPPR high-^{240}Pu
fuel experiments and the results obtained in previous criticals
experience is considered.

I. INTRODUCTION

The effect of plutonium isotopic composition on criticality and other key
reactor parameters was measured in ZPPR assembly 4. ZPPR assembly 4 was part
of the DEMO Benchmark series of critical experiments for the Demonstration
Breeder Reactor. Normal ZPPR fuel was replaced by high-^{240}Pu (H240) fuel in
a sector which occupied approximately 10% of the core volume. Criticality was
achieved by adjusting fuel spikes within the sector until the excess reacti-
vity of the reference configuration was matched. The ^{239}Pu(n,f) reaction rate
across the sector was also matched to that of the reference configuration.
Measurements in the H240 zone, which were exactly repeated in the correspond-
ing reference configuration, included small sample reactivity worths, pluton-
ium and uranium reaction rates, a control rod substitution worth, sodium void
worth, and the ^{238}U Doppler effect.

Analysis of most of the experiments was done with two-dimensional diffu-
sion theory. The ability of the standard analysis techniques to predict
changes caused by the H240 fuel was of central interest. The fuel composition
of the Clinch River Breeder Reactor (CRBR) will undoubtedly be different from
that of the DEMO Benchmark, ZPPR assembly 4. Hence, it is essential to know
how calculated-to-experimental (C/E) ratios vary with changes in fuel composi-
tion.

A similar series of experiments with the H240 fuel was performed in ZPR-
6 assembly 7 [1]. These measurements were all made in a central zone of the
same composition as the ZPPR assembly 4 inner core. No control rods were in
the zone. By contrast, the ZPPR experiments were designed to measure the
effects of the H240 fuel in the outer core and with control rods present.

II. CONFIGURATION

The configuration for the H240 plutonium experiment is presented in Fig.
1. The initial core, beginning-of-cycle (IC-BOC) configuration for the CRBR
was simulated. Control rods were fully inserted in the central position and
in the outer ring flats. These type N-1 control rods (CRs) are fully de-
scribed in ANL-RDP-25 [2,3]. Other control positions (CRPs) are filled with
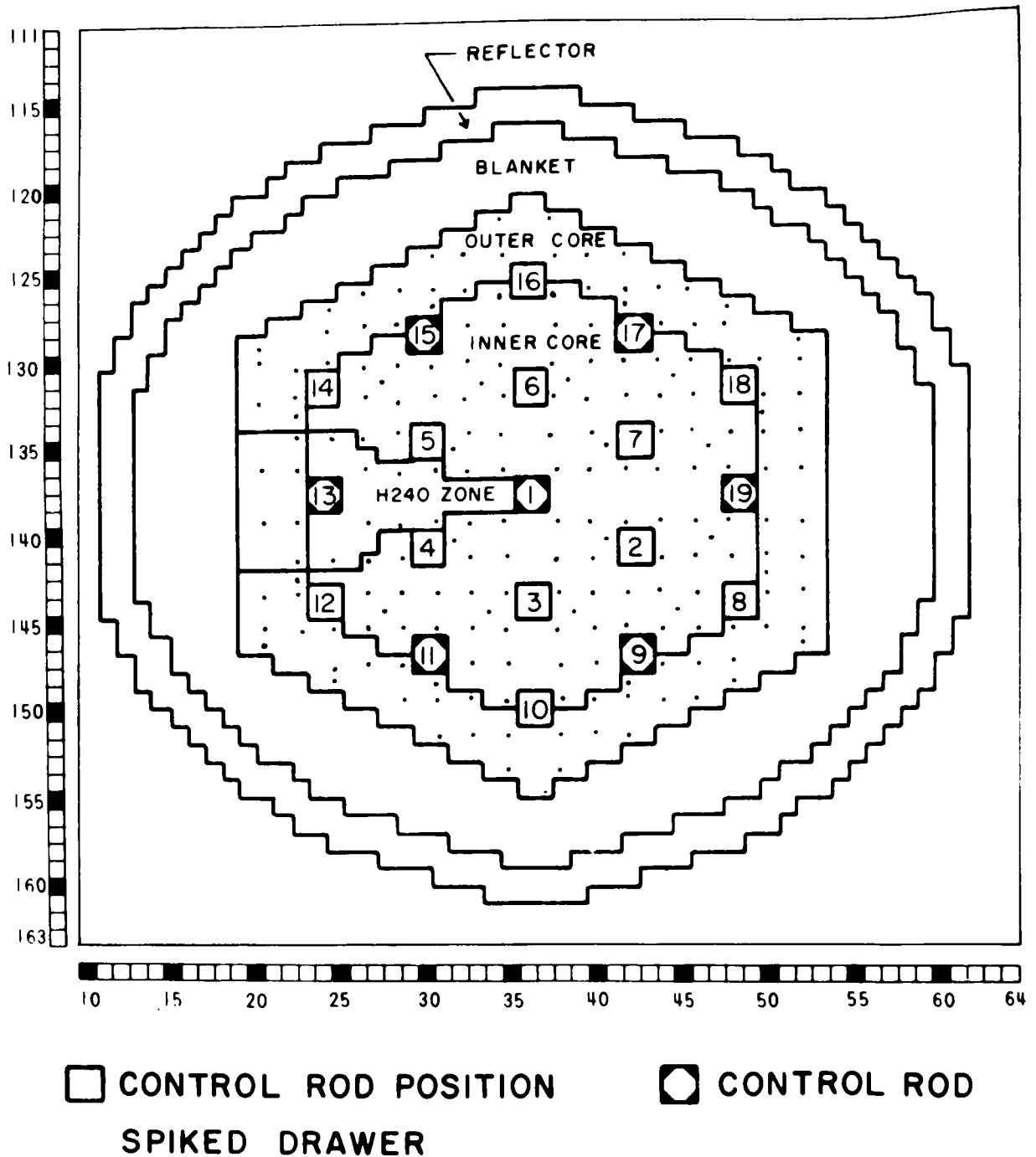
Fig. 1. The ZPPR Assembly 4, Phase 2 IC-BOC Configuration
with the High-^{240}Plutonium Sector

sodium and steel. Criticality was adjusted by the addition of the distributed
fuel spikes [4] that are indicated in Fig. 1. The normal configuration (with-
out the H240 fuel) was symmetric about the x, y, and z axes. For that config-
uration [5,6,7] the spiking pattern can be inferred from the upper right-hand
quadrant of Fig. 1.

Unit cells for the different zones of the reactor are presented in Fig.
2. In the H240 sector, high-^{240}Pu was substituted for the normal ZPPR Pu fuel
plates. The composition of normal ZPPR Pu fuel and high-^{240}Pu fuel are com-
pared in Table I. The principal things to note regarding the compositions
are: (1) the combined mass of ^{239}Pu + ^{241}Pu is the same for both fuel types,
(2) the normal ZPPR fuel has 11.5% ^{240}Pu while the high-^{240}Pu fuel has 26.0%
^{240}Pu, (3) the percentage of ^{238}U is reduced in the H240 fuel to allow for the
additional ^{240}Pu. Each of the above contributes to making the H240 fuel more
reactive than the normal fuel. This results from (1) the ratio of ^{241}Pu to
^{239}Pu being greater in the H240 fuel and (2) ^{238}U, which has a negative reac-
tivity in the core, being replaced by ^{240}Pu, which has a positive reactivity
in the core.

Three criteria were selected for defining the replacement of normal ZPPR
fuel by H240 fuel in one sector of the reactor. These criteria were (1) that
the ^{239}Pu(n,f) reaction rate measured across row 137 remain constant, (2) that
the system excess reactivity change as little as possible and (3) that all
fuel in the sector be of the H240 type. It was not self-evident that all
three criteria could be met since the number and the location of the fuel
spikes were the only variables.

With the spiking pattern shown in Fig. 1, the excess reactivity for the
H240-zoned core was 6.8 ± 0.2 x 10^{-4} Δk/k. For the normal core the excess
reactivity had been 6.5 ± 0.2 x 10^{-4} Δk/k. These numbers are not adjusted
for differences in temperature and half closure. Since the spikes were worth
an average of 0.15\$ per column, this difference of less than 0.01\$ in excess
reactivity was considered to have suitably met the second criterion.

The ^{239}Pu(n,f) reaction rate was measured across row 137 (which bisects
the sector) prior to the installation of the H240 fuel. The measurement was
made by traversing a fission chamber in a slot created by adjusting the
drawers at the reactor midplane. After loading the H240 fuel and adjusting
criticality, the measurement was repeated. The shape of the ^{239}Pu(n,f) tra-
verse across row 137 was discovered to have remained relatively unchanged.
Results of the two traverses are presented in Fig. 3. Both traverses were
normalized to a stationary fission chamber in matrix position 237-50. From
Fig. 3 it is readily evident that the plutonium fission rate in row 137 is
the same for both cores. Hence, the first criterion for establishment of the
H240 sector was met.

Satisfying all three criteria for the H240 sector resulted in placing six
fewer fuel spikes in the sector than had been there in the normal configura-
tion. In terms of zone enrichment this meant a reduction in the fissile to
heavy metal ratio of 4.4% for the inner core and 3.3% for the outer core.
These numbers correspond favorably to high-^{240}Pu reactivity measurements made

TABLE I. Comparison of Normal and H240
Fuel Plate Composition

Component	Normal ZPPR Fuel Composition		High ^{240}Pu Fuel Composition	
	Wt.%	% Pu	Wt.%	% Pu
^{238}Pu	0.02	0.07	0.03	0.09
^{239}Pu	24.46	86.68	23.18	67.60
^{240}Pu	3.25	11.52	8.90	25.96
^{241}Pu	0.44	1.56	1.70	4.95
^{242}Pu	0.05	0.17	0.48	1.40
^{241}Am [a]	0.09	- -	0.09	- -
^{238}U	69.03	- -	63.07	- -
^{235}U	0.15	- -	0.14	- -
Mo	2.51	- -	2.41	- -

[a]Decay corrected to January 1, 1971.
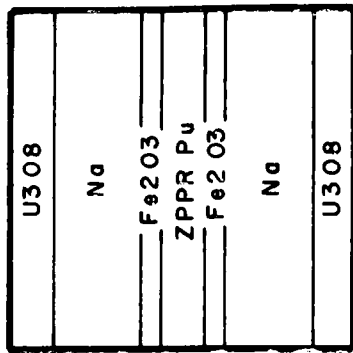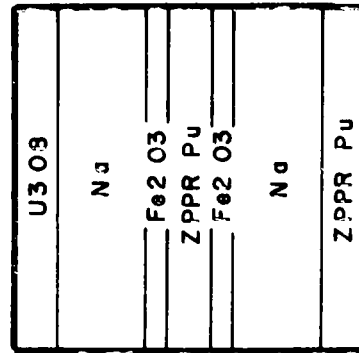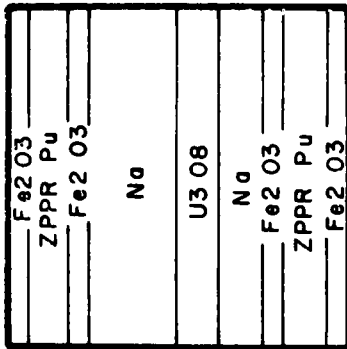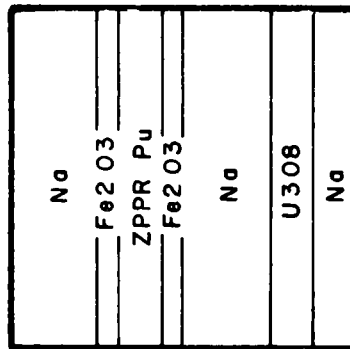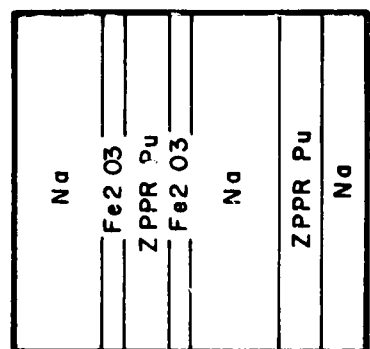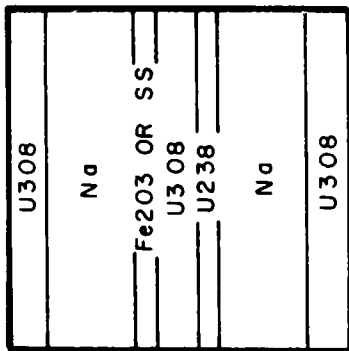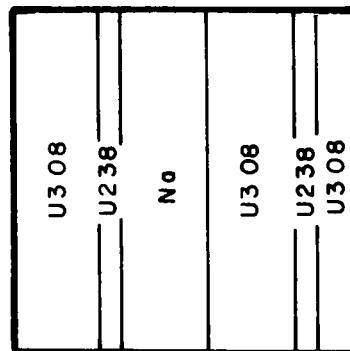
Fig. 2. Unit Cells Used in ZPPR Assembly 4.
Drawer Front View, Half No. 1 Left Side.
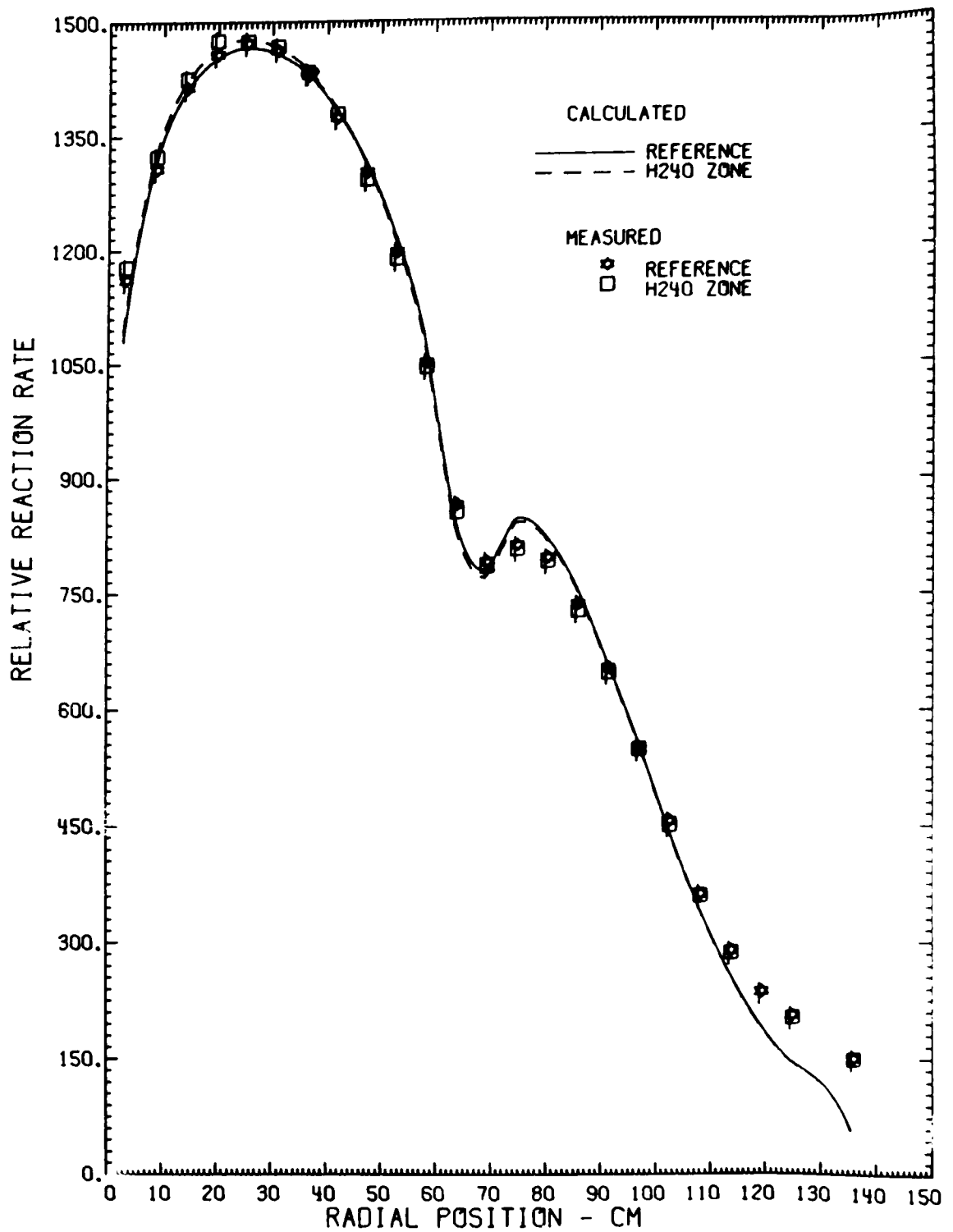
Fig. 3. Results of the ^{239}Pu Fission Counter Traverse Across Row 137 in the Reference and the H240-Zoned Cores.

in ZPPR assembly 2 [8] and in ZPR-6 assembly 7 [9]. This is not surprising since each of the latter two assemblies were also in the DEMO Benchmark series.

III. DESCRIPTION OF CALCULATIONS

The SDX [10] package and ENDF/B Version III data libraries were used to generate the 28-group cross sections used in this study. Resonance hetero-geneity was based on a one-dimension representation of the cells shown in Fig. 2. Cell cross sections were generated for the normal and voided conditions for both the high-^{240}Pu cells and the standard cells.

All calculational models were based on as-built dimensions and material loadings. Radial zone boundaries for the r and rz models were chosen to con-serve the assembly 4 region volumes. Axial dimensions were the same as the as-built zone heights. The xy model had one mesh interval per drawer so that each drawer type could be represented explicitly. The rz and xy calculational models are shown in Figs. 4, 5, and 6. Homogeneous drawer compositions and volume fractions for the various models are shown in Tables II, III, IV, and V. Uncertainties in number densities are on the order of one percent.

The ARC system standard paths 3 and 7 [11,12] diffusion and perturbation modules, were used to produce k_{eff} values, flux distributions and delayed neu-tron data. First order perturbation (FOP) worth scans were generated with PERT-V [13] while a TOPSY [14] calculation provided the reaction rate scans and group and region dependent leakage corrections.

The sequence of calculations began with the rz models. Although the azi-muthal assymetries were not represented explicitly, zone volumes and loadings were conserved so that an average azimuthal behavior was calculated. Results of the rz calculation were used for the perturbation denominator and reaction rate integrals. Leakage correction and normalizations for r and xy calcula-tions were also provided from this computation. Leakage terms as generated from the IC-BOC rz fluxes were applied to both the IC-BOC and the H240 r and xy models. An rz model was run for the H240 core to account for isotopic changes on the value of β_{eff}. The delayed data are shown in Tables VI and VII for the two phase-2 core loadings. An r model was run for the IC-BOC core to generate the normalization for the radial perturbation worths. The same factor was applied to both phase-2 core calculations.

A 1/4-core xy model was used for the IC-BOC core, while a 1/2-core model was needed for the H240-zoned core. These models, both with the same group and region dependent leakage corrections, were used to predict radial reaction rates and small-sample perturbation worth distributions. Corrections to zero-size worths for comparison with measured worths of the small samples were gen-erated using the SARCASM code.

For the off-center control rod interchange worth and the sodium-voiding predictions, a 1/2-core xy model was run for both core configurations. Both of these calculations used a constant buckling treatment which gave the same k_{eff} value as the xy calculation discussed above. The rod worths were taken from the difference in k_{eff}. Sodium-voiding worth predictions were taken from
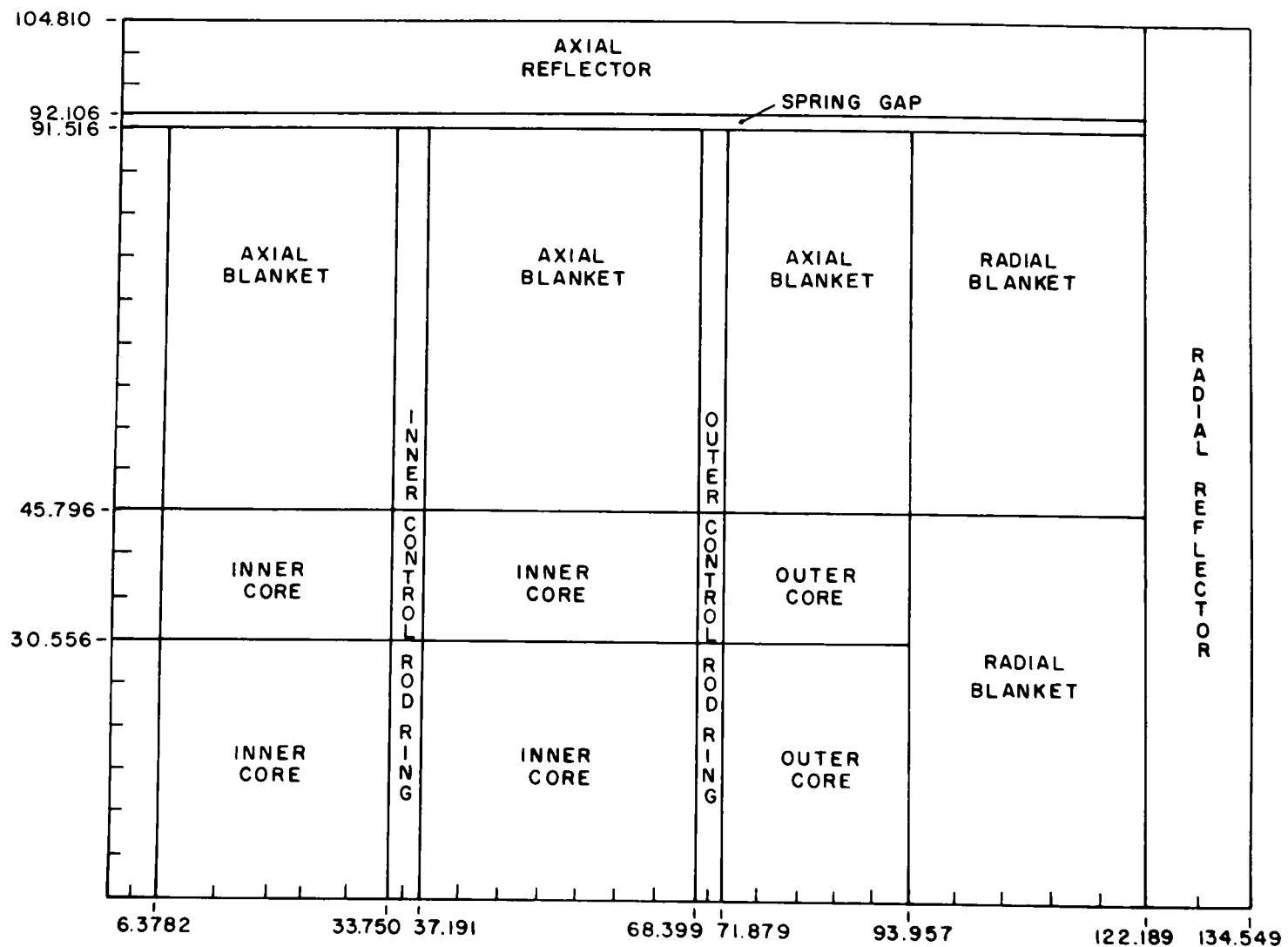
Fig. 4. rz Model of ZPPR Assembly 4, Phase 2.
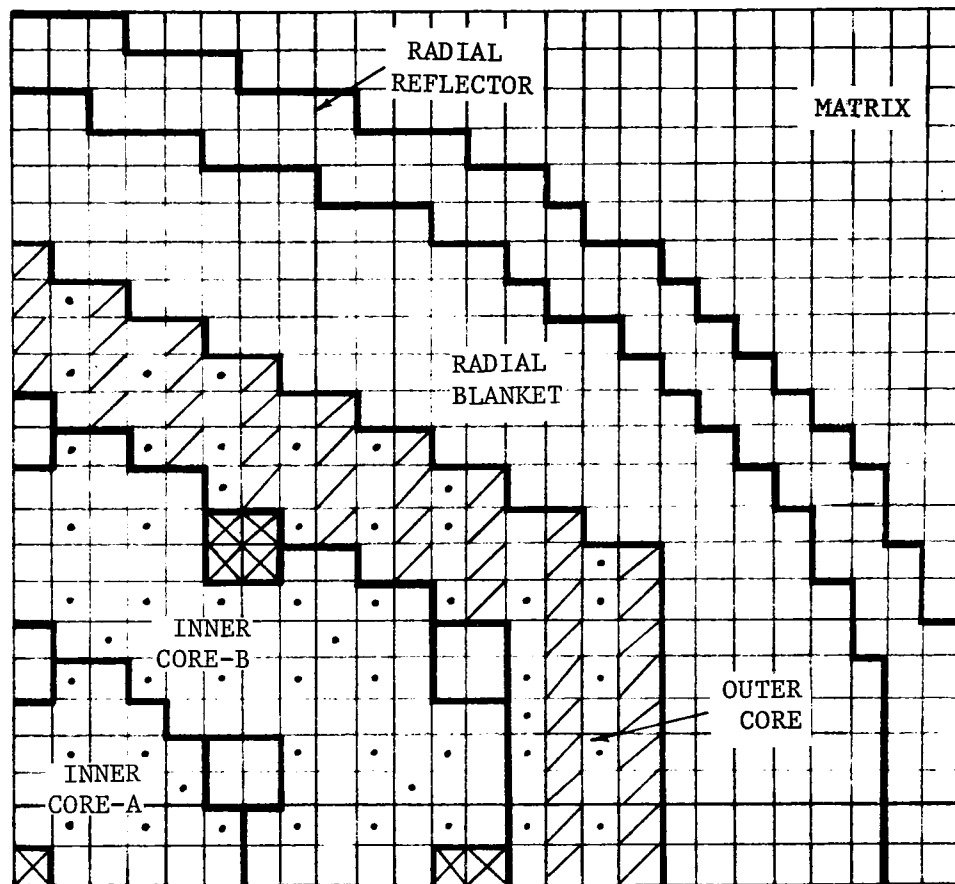
Fig. 5. Phase 2 IC-BOC Reference Configuration

SODIUM FILLED CRP

SPIKED DRAWER

TYPE -A DRAWER

B$_4$C LOADED CR

$\Delta Y=5.7836$ cm

$\Delta X=5.5245$ cm

RADIAL REFLECTOR

MATRIX

RADIAL BLANKET

INNER CORE-B

OUTER CORE

INNER CORE-A

9
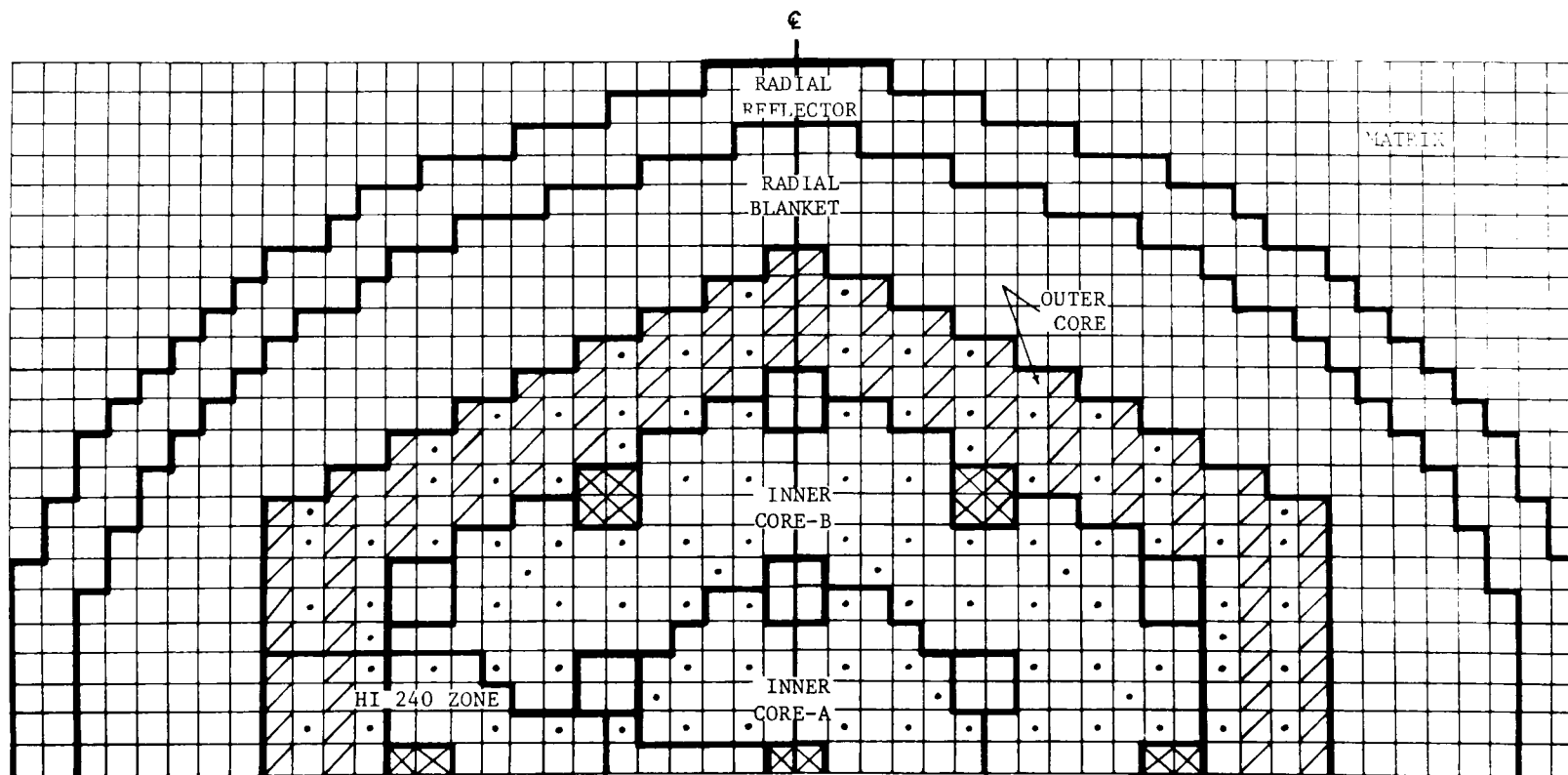
SODIUM FILLED CRP

SPIKED DRAWER

TYPE-A DRAWER

B_4C LOADED CR

$\Delta Y = 5.7836$ cm

$\Delta X = 5.5245$ cm

Fig. 6. Phase 2 HI ^{240}Pu-Zoned Core.

TABLE II. Homogenized Drawer Compositions for ZPPR Assembly 4 ($\times 10^{22}$) Normal Core

	Inner Core Normal	Inner Core Spiked	Outer Core Type A	Outer Core Type B	Outer Core Spiked	Radial Blanket	Radial Reflector	Axial[c] Blanket (SS)	Axial[c] Blanket (Fe$_2$O$_3$)	Axial Reflector
^{239}Pu	0.08439	0.16895	0.16893	0.08452	0.16904					
^{240}Pu[a]	0.01123	0.02250	0.02250	0.01124	0.02249					
^{241}Pu[b]	0.00130	0.00260	0.00260	0.00130	0.00258					
^{242}Pu	0.00018	0.00036	0.00037	0.00018	0.00036					
^{241}Am[b]	0.00053	0.00110	0.00105	0.00053	0.00106					
^{235}U	0.00123	0.00142	0.00142	0.00088	0.00107	0.00279		0.00156	0.00156	
^{238}U	0.55533	0.63657	0.63695	0.39761	0.47921	1.26574		0.70605	0.70605	
Na	0.88641	0.88641	0.63976	1.08557	1.08557	0.44705		0.88877	0.88789	
O	1.31295	0.89192	1.45144	0.89208	0.47105	2.13512		1.26518	1.52694	
Fe	1.22993	1.32165	1.68182	1.30983	1.40126	0.72080	7.13450	1.10665	0.98960	7.15655
Cr	0.26089	0.28757	0.28405	0.28428	0.31089	0.20605	0.11924	0.31461	0.23321	0.12052
Ni	0.11893	0.13230	0.13057	0.13058	0.14394	0.09151	0.05133	0.14184	0.10509	0.05133
Mn	0.02193	0.02386	0.02361	0.02363	0.02555	0.01796	0.05860	0.02790	0.01992	0.05981
Mo	0.02357	0.04530	0.04522	0.02364	0.04529	0.00185	0.00118	0.00193	0.00192	0.00118
C	0.00292	0.00292	0.00292	0.00292	0.00292	0.00292	0.05771	0.00424	0.00291	0.05576
Al	0.00034	0.00046	0.00044	0.00043	0.00053	0.00011	– –	0.00021	0.00023	– –
Si	0.01307	0.01435	0.01417	0.01422	0.01551	0.01043	0.00684	0.01626	0.01172	0.00503
P	0.00046	0.00046	0.00046	0.00046	0.00046	0.00046	0.00176	0.00076	0.00046	0.00155
S	0.00016	0.00016	0.00016	0.00016	0.00016	0.00016	0.00275	0.00024	0.00016	0.00249
Co	0.00036	0.00036	0.00036	0.00036	0.00036	0.00036	– –	0.00035	0.00035	– –
Cu	0.00287	0.00303	0.00301	0.00301	0.00317	0.00254	0.00126	0.00270	0.00270	0.00126

TABLE II. (cont'd)

	Spring[d] Gap	Core CRP	Blanket CRP	Boron Rod Nat.(N-1)	Boron Rod Pseudo 50% Enriched (M)	Boron Rod Type A	Boron Rod Type I
Na	– –	1.77718	1.74851	0.82206	0.37907	1.33288	0.60196
O	– –	– –	– –	0.00486	0.00880	– –	0.00973
Fe	3.09933	1.00239	1.01707	1.18189	0.86249	1.05752	1.02798
Cr	0.72477	0.28795	0.29232	0.33504	0.24435	0.30178	0.29107
Ni	0.31499	0.13228	0.13457	0.15198	0.11065	0.13727	0.13197
Mn	0.05390	0.02387	0.02420	0.02937	0.02071	0.02592	0.02516
Mo	0.00372	0.00208	0.00209	0.00200	0.00197	0.00201	0.00197
C	0.03720	0.00292	0.00290	0.82869	1.50512	0.44088	1.22596
Al	– –	0.00043	0.00049	0.00027	0.00026	0.00032	0.00032
Si	0.04724	0.01432	0.01454	0.02062	0.01890	0.01636	0.02142
P	0.00159	0.00045	0.00046	0.00076	0.00046	0.00061	0.00061
S	0.00063	0.00016	0.00016	0.00024	0.00016	0.00020	0.00020
Co	0.00151	0.00036	0.00035	0.00036	0.00036	0.00036	0.00036
Cu	0.00602	0.00303	0.00306	0.00283	0.00278	0.00287	0.00281
^{10}B	– –	– –	– –	0.63904	1.16420	0.33327	0.95331
^{11}B	– –	– –	– –	2.59132	4.72102	1.35112	3.86569

[a] ^{240}Pu = ^{240}Pu + ^{238}Pu.

[b] Adjusted to 1/1/74.

[c] Average of inner and outer axial blanket region.

[d] Between 915.162 and 921.055 mm in 914.4 mm drawers.

TABLE III. Homogenized Drawer Compositions for High-^{240}Pu Fuel Zone Experiment in ZPPR Assembly 4 Number Density, 10^{22} atoms/cm^3.

Material	Inner Core Normal	Inner Core Spiked	Outer Core Type A	Outer Core Type B	Outer Core Spiked
^{239}Pu	0.07983	0.15978	0.15991	0.08001	0.15970
^{240}Pu[a]	0.03078	0.06156	0.06156	0.03077	0.06155
^{241}Pu[b]	0.00491	0.00981	0.00978	0.00488	0.00981
^{242}Pu	0.00167	0.00332	0.00332	0.00165	0.00333
^{241}Am[b]	0.00164	0.00327	0.00326	0.00161	0.00326
^{235}U	0.00118	0.00133	0.00133	0.00084	0.00098
^{238}U	0.53491	0.59596	0.59601	0.37707	0.43781
Na	0.87926	0.88641	0.63976	1.08557	1.08557
O	1.31295	0.89192	1.45144	0.89208	0.47105
Fe	1.23037	1.32231	1.68121	1.30980	1.40137
Cr	0.26084	0.28755	0.28375	0.28426	0.31048
Ni	0.11887	0.13231	0.13042	0.13057	0.14375
Mn	0.02192	0.02387	0.02360	0.02364	0.02553
Mo	0.02294	0.04397	0.04396	0.02300	0.04403
C	0.00292	0.00292	0.00292	0.00292	0.00292
Al	0.00033	0.00045	0.00044	0.00044	0.00056
Si	0.01305	0.01437	0.01417	0.01422	0.01549
P	0.00046	0.00046	0.00046	0.00046	0.00046
S	0.00016	0.00016	0.00016	0.00016	0.00016
Co	0.00035	0.00036	0.00036	0.00036	0.00036
Cu	0.00286	0.00303	0.00301	0.00301	0.00316

[a]^{240}Pu = ^{240}Pu + ^{238}Pu.

[b]As of January 1, 1974.

TABLE IV. Drawer Volume Fractions for ZPPR Assembly 4,
Phase 2 IC-BOC.

Inner Core	
Normal Cell	0.74074
Spiked Cell	0.25926
Outer Core	
Normal 2 Drawer Cell	
Type A Drawer	0.211111
Type B Drawer	0.211111
Spiked 2 Drawer Cell	
Type A Drawer	0.266667
Type B Drawer[a]	0.266667
Single Drawer Cell	
Type A Drawer	0.044444
Axial Blanket	
SS Column	0.5
Fe_2O_3 Column	0.5
Outer Control Ring	
Na Channels	0.5
Control Rod Type N	0.4

[a]The spike is in the B Drawer only.

TABLE V.   Drawer Volume Fractions for ZPPR
            Assembly 4, Phase 2 High ^{240}Pu
            Sector Core

Inner Core	
Normal Cell	0.65278
Spiked Cell	0.23148
High ^{240}Pu Normal Cell	0.09722
High ^{240}Pu Spiked Cell	0.01852
Outer Core	
Normal 2 Drawer Cell	
Type A Drawer	0.188889
Type B Drawer	0.188889
Spiked 2 Drawer Cell	
Type A Drawer	0.244444
Type B Drawer[a]	0.244444
High ^{240}Pu Normal 2 Drawer Cell	
Type A Drawer	0.027778
Type B Drawer	0.027778
High ^{240}Pu Spiked 2 Drawer Cell	
Type A Drawer	0.016667
Type B Drawer[a]	0.016667
Single Drawer Cell	
Type A Drawer	0.044444
Axial Blanket	
SS Column	0.5
Fe_2O_3 Column	0.5
Outer Control Ring	
Na Channels	0.5
Control Rod Type N	0.4

[a]The spike is in the type B drawer only.

TABLE VI. Delayed Data for ZPPR Assembly 4, Phase 2 IC-BOC
Using ENDF/B Version 4 Delayed Data

	Effective Delayed Neutron Fractions, 10^{-3}/Reactor Fission						
	Precursor Group						
Isotope	1	2	3	4	5	6	Total
^{235}U	0.002168	0.012881	0.011157	0.024675	0.007760	0.001576	0.060218
^{238}U	0.018529	0.204998	0.238559	0.582051	0.337530	0.112510	1.49418
^{239}Pu	0.056866	0.438206	0.333062	0.514628	0.161606	0.054915	1.55928
^{240}Pu	0.001677	0.017102	0.011851	0.021982	0.008039	0.001821	0.062473
^{241}Pu	0.000706	0.018010	0.013366	0.030672	0.014348	0.001283	0.078385
^{242}Pu	0.000004	0.000320	0.000301	0.000684	0.000295	0.000242	0.001883
Total	0.079988	0.691517	0.608297	1.17469	0.529578	0.172347	3.25642
Average Decay Constant, sec^{-1}/	0.01296	0.03137	0.13520	0.34401	1.36532	3.71550	

Total β_{eff} = 0.003256

Prompt Lifetime = 4.313 x 10^{-7} sec

Inhours per % $\Delta k/k$ = 993.9

TABLE VII. Delayed Data for ZPPR Assembly 4, Phase 2 High-^{240}Pu
Sector Core Using ENDF/B Version 4 Delayed Data

	Effective Delayed Neutron Fractions, 10^{-3}/Reactor Fission						
	Precursor Group						
Isotope	1	2	3	4	5	6	Total
^{235}U	0.002155	0.012809	0.011094	0.024540	0.007718	0.001568	0.059884
^{238}U	0.018411	0.203753	0.237085	0.578593	0.335524	0.111841	1.48521
^{239}Pu	0.051659	0.432874	0.328975	0.508435	0.159661	0.054254	1.54036
^{240}Pu	0.001957	0.019957	0.013828	0.025654	0.009382	0.002126	0.072903
^{241}Pu	0.000896	0.022866	0.016969	0.038949	0.018220	0.001629	0.099529
^{242}Pu	0.000075	0.000579	0.000543	0.001236	0.000533	0.000437	0.003402
Total	0.079654	0.692837	0.608493	1.17741	0.531038	0.171855	3.26129
Average Decay Constant, sec^{-1}/	0.01296	0.03137	0.13520	0.34401	1.36532	3.71550	

Total β_{eff} = 0.003261

Prompt Lifetime = 4.307 x 10^{-7} sec

Inhours per % $\Delta k/k$ = 992.9

FOP calculations using the xy flux distributions of the constant buckling models. Axial flux distributions defined by cos Bz, where B^2 is the buckling value, were used to accomplish 12 in. and 18 in. axial integrations of the FOP worth.

IV. REACTIVITY MEASUREMENTS

Four basic types of reactivity measurements were made for comparison between the normal and the high-^{240}Pu zoned core. These were: (1) radial reactivity traverses of small samples of important reactor materials, (2) measurement of the sodium-void reactivity in a 4 x 4 drawer outer-core zone, (3) a control rod substitution measurement in CRP-13 and (4) measurement of the ^{238}U Doppler coefficient in the outer core zone. Since similar measurements had been made near the center of ZPR-6 assembly 7, the outer core was emphasized in the ZPPR assembly 4 measurements.

Where possible we have included calculations in support of these measurements. The calculations were of central interest because of the importance placed on extrapolating the results of ZPPR measurements to what they would be with a different fuel composition. One of the most compelling reasons for doing the experiments was to demonstrate that reactivity changes resulting from the H240 substitution could be predicted by standard calculational procedures.

A. Small-Sample Reactivity Measurements and Calculations

Small-sample reactivity traverses were made in the slot (row 137, see Fig. 1) at the reactor midplane in both the normal core [15] and the H240-zoned core [16]. Samples included in the measurement were ^{239}Pu, ^{240}Pu, ^{241}Pu, ^{235}U, ^{238}U, ^{10}B and stainless steel. Compositions and descriptions of the samples are found in Table VIII.

The samples were oscillated between the edge of the matrix and the center of the core. During the oscillation the samples were stopped for 10 seconds at the center of each blanket, core and CR drawer encountered along the traverse. The hold time at the endpoints was 60 seconds. For a more detailed description of the experimental technique employed at ZPPR, see Ref. 17.

Sample position and reactor power data were collected by the SEL-840 computer. Inverse-kinetics analysis was used to obtain reactivity versus position values for each sample. These values were corrected for power drift during the run by a third-order drift fit. Corrections were made for the reactivity due to the sample capsule and drive mechanism. This was accomplished by subtracting values measured while traversing an empty capsule.

Calculation of the measured set of reactivities required a lengthy procedure. FOP values of the isotopic worths were computed with the PERT-V code. The required input cross sections and flux sets were generated as described above (see p. 7 this report). The isotopic worths were combined appropriately for the sample compositions. This was done at 23 radial locations. Subsequently, the pointwise values were numerically averaged over the physical length of the sample. As a final step these reactivities were corrected for

TABLE VIII.   Description of Reactivity Samples Used in ZPPR
Assembly 4, Phase 2

Sample	Dimensions, cm		Sample mass, g	Capsule mass, g	Principal Composition	
	Length	O.D.			Component	Wt.%
Pu-30	5.519	0.762	38.091	11.600	^{239}Pu	98.03
					^{240}Pu	1.01
					Al	0.96
Pu-50	0.399	0.533	0.582	17.528	^{239}Pu	1.02
					^{240}Pu	2.72
					$^{241}Pu^a$	69.72
					^{242}Pu	1.36
					$^{241}Am^a$	13.00
					O	12.18
P240-R	4.775	0.836	13.776	10.222	^{239}Pu	0.92
					^{240}Pu	82.29
					$^{241}Pu^b$	0.50
					^{242}Pu	4.08
					O	12.21
U-6	5.519	0.762	46.889	11.463	^{234}U	0.95
					^{235}U	93.19
					^{236}U	0.26
					^{238}U	5.60
DU-6	5.519	0.762	47.427	11.417	^{235}U	0.213
					^{238}U	99.787
SS-1	5.519	0.991	33.635	10.347	Fe	70.47
					Cr	19.08
					Ni	8.64
					Mn	1.41
					Si	0.30
					Cu	0.10
B-1	5.519	1.019	4.193	10.521	^{10}B	89.92
					^{11}B	7.62
					O	1.48
					C	0.99

[a]Reference for date decay of ^{241}Pu is June 1969.

[b]Reference for date decay of ^{241}Pu is Jan. 1974.

finite sample size by self-shielding factors generated via the SARCASM [18]
procedure. Except for the effects due to the slot and the extra steel in the
push and follower rods, the calculated reactivities then corresponded to the
measured reactivities on a one-to-one basis.

Results of the reactivity traverse measurements are presented in Tables
IX – XV and are displayed in Figs. 7-13. In the figures, the ever-present
central worth discrepancy has been normalized out. The required normalization
factor is given by the average C/E ratio tabulated on the figure. From the
standpoint of comparative measurements, very little difference is observed be-
tween the results in the H240 sector and the normal core results. The magni-
tude of the sample reactivities increased very slightly in the inner core when
the H240 sector was installed. This was well predicted by the calculations.
The scatter in the Pu-50 and the SS-1 measurements is primarily due to the
large size of the drift correction relative to the sample reactivity. The
extremely small mass of the ^{241}Pu sample makes accurate measurement of its
reactivity almost impossible.

In ZPR-6 assembly 7, the average ratio of sample central worths in the
H240 zone to central worths in the reference core was 1.11 [1]. This ratio
is very close to 1.0 for the H240 experiments in ZPPR assembly 4. In ZPR-6
almost all of the increase in worth was ascribed to a change in the perturba-
tion denominator and changes in the local flux profiles. In ZPPR assembly 4,
the calculated perturbation denominators were the same to within 0.5%. Al-
though a measured value is not available, the small calculated difference in
perturbation denominators seems quite reasonable because of the way the zone
was loaded. The ZPR-6 H240 zone was accomplished by plate for plate substi-
tution with criticality adjustment by spike manipulation at the edge of the
core. This method of loading resulted in the substantial perturbation denomi-
nator change.

At least two results of the study of the effect of Pu composition on
small-sample reactivities were significant. The first is that, as expected,
only very minor changes were observed in the measured reactivities despite
the significant alteration of the plutonium isotopic balance. The second is
that the C/E ratios calculated for the samples in both the H240 case and the
normal case were very close. The average C/E did increase about 2% in the
H240 case, but the reactivity profiles were equally well calculated. As dis-
cussed above, the perturbation-denominator normalization for the IC-BOC was
applied to both the normal and the H240 calculations. This may have contri-
buted to the 2% bias in C/E values.

B.   Sodium-Void Reactivity Measurements and Calculations

Sodium-void reactivity was measured in a 4 x 4 drawer zone of the outer
core. The zone was voided over two different axial heights in both the normal
core and the H240-zoned core. Identical procedures were used in both sets of
measurements. Location of the voided zone within the H240 sector is shown in
Fig. 14.

Removal of the sodium consisted of replacing sodium-filled steel cans
with empty steel cans. In the first step this substitution took place in the

TABLE IX. Results of the Pu-30 (^{239}Pu) Radial Reactivity Traverse

Zone	Position, cm	Reference Core Measured Worth, Ih/kg	C/E	H240-Zoned Core Measured Worth, Ih/kg	C/E
Control Rod	2.764	97.1 ± 0.1		98.5 ± 0.1	1.05
Inner Core	8.288	107.8 ± 0.1	1.08	110.2 ± 0.1	1.08
	13.813	113.8 ± 0.1	1.09	115.6 ± 0.1	1.10
	19.337	114.9 ± 0.1	1.11	117.2 ± 0.1	1.12
	24.862	113.0 ± 0.1	1.12	115.5 ± 0.1	1.13
	30.386	109.4 ± 0.1	1.13	111.2 ± 0.1	1.15
	35.911	104.6 ± 0.1	1.14	105.0 ± 0.1	1.16
	41.435	97.7 ± 0.1	1.16	98.4 ± 0.1	1.17
	46.960	90.3 ± 0.1	1.16	89.6 ± 0.1	1.18
	52.484	80.7 ± 0.1	1.17	79.2 ± 0.1	1.19
	58.009	68.6 ± 0.1	1.17	67.2 ± 0.1	1.19
Control Rod	63.533	54.2 ± 0.1	1.15	52.3 ± 0.1	1.17
Control Rod	69.058	46.5 ± 0.1	1.13	44.9 ± 0.1	1.16
Outer Core	74.582	43.5 ± 0.1	1.18	42.3 ± 0.1	1.21
	80.107	38.8 ± 0.1	1.20	38.4 ± 0.1	1.22
	85.631	32.3 ± 0.1	1.18	32.0 ± 0.1	1.20
	91.156	24.4 ± 0.1	1.18	24.5 ± 0.1	1.19
Radial Blanket	96.680	16.8 ± 0.1	1.15	16.6 ± 0.1	1.17
	102.205	10.6 ± 0.3	1.11	11.0 ± 0.3	1.06
	107.729	6.5 ± 0.3	1.02	6.5 ± 0.3	1.01
	113.254	3.5 ± 0.3	1.02	3.5 ± 0.3	1.02
	118.778	2.0 ± 0.3	0.92	1.5 ± 0.3	1.30
	124.303	1.9 ± 0.3	0.51	0.2 ± 0.3	
Reflector	129.827	1.2 ± 0.3	0.40	0.1 ± 0.3	
Reflector	135.352	0.7 ± 0.3		-0.2 ± 0.3	
Matrix	140.876	-0.3 ± 0.3		-0.3 ± 0.3	
Matrix	146.401	0.1 ± 0.1		0.0 ± 0.1	

TABLE X.   Results of the P240R (^{240}Pu) Radial Reactivity Traverse

Zone	Position, cm	Reference Core Measured Worth, Ih/kg	C/E	H240-Zoned Core Measured Worth, Ih/kg	C/E
Control Rod	2.764	8.7 ± 0.2		8.8 ± 0.1	1.12
Inner Core	8.288	12.3 ± 0.2	0.99	12.4 ± 0.2	1.00
	13.813	12.6 ± 0.2	0.99	12.4 ± 0.2	1.05
	19.337	12.0 ± 0.2	1.05	12.1 ± 0.2	1.10
	24.862	12.4 ± 0.2	1.00	13.1 ± 0.2	1.00
	30.386	11.4 ± 0.2	1.06	11.7 ± 0.2	1.09
	35.911	11.3 ± 0.2	1.02	11.5 ± 0.2	1.06
	41.435	10.5 ± 0.2	1.07	11.4 ± 0.2	1.04
	46.960	10.5 ± 0.2	1.01	10.7 ± 0.2	1.04
	52.484	9.8 ± 0.2	1.04	9.8 ± 0.1	1.06
	58.009	9.6 ± 0.2	0.97	9.2 ± 0.2	1.00
Control Rod	63.533	5.9 ± 0.2	1.16	5.6 ± 0.1	1.15
Control Rod	69.058	4.3 ± 0.2	1.24	4.3 ± 0.2	1.20
Outer Core	74.582	5.3 ± 0.3	1.13	5.3 ± 0.2	1.13
	80.107	5.6 ± 0.2	1.11	5.5 ± 0.2	1.14
	85.631	4.8 ± 0.2	1.10	5.4 ± 0.2	1.00
	91.156	4.5 ± 0.2	0.91	4.9 ± 0.2	0.87
Radial Blanket	96.680	2.3 ± 0.2	0.89	3.2 ± 0.2	0.70
	102.205	1.8 ± 0.5	0.51	1.4 ± 0.5	0.70
	107.729	1.5 ± 0.5		0.7 ± 0.5	0.67
	113.254	-0.1 ± 0.6	2.27	0.6 ± 0.5	
	118.778	0.1 ± 0.5	0.71	0.5 ± 0.5	
	124.303	1.0 ± 0.7		0.6 ± 0.5	0.65
Reflector	129.827	0.1 ± 0.5		0.3 ± 0.6	1.48
Reflector	135.352	-0.1 ± 0.5		0.2 ± 0.5	
Matrix	140.876	-0.4 ± 0.5		-0.6 ± 0.6	
Matrix	146.401	0.0 ± 0.1		0.0 ± 0.1	

TABLE XI. Results of the Pu-50 (^{241}Pu) Radial Reactivity Traverse

Zone	Position, cm	Reference Core Measured Worth, Ih/kg		C/E	H240-Zoned Core Measured Worth, Ih/kg		C/E
Control Rod	2.764	87	± 4		77	± 4	1.21
Inner Core	8.288	104	± 6	1.05	119	± 6	0.94
	13.813	124	± 7	0.94	114	± 8	1.05
	19.337	131	± 7	0.92	104	± 7	1.18
	24.862	89	± 7	1.35	116	± 7	1.06
	30.386	84	± 6	1.39	109	± 6	1.10
	35.911	112	± 7	1.00	74	± 7	1.54
	41.435	66	± 7	1.62	75	± 7	1.45
	46.960	74	± 7	1.33	73	± 6	1.36
	52.484	54	± 6	1.64	79	± 7	1.11
	58.009	55	± 7	1.38	57	± 6	1.33
Control Rod	63.533	69	± 6	0.81	43	± 7	1.29
Control Rod	69.058	39	± 6	1.19	47	± 6	0.99
Outer Core	74.582	40	± 5	1.17	0	± 6	
	80.107	32	± 7	1.33	19	± 6	2.21
	85.631	27	± 7	1.31	9	± 6	
	91.156	19	± 6	1.42	26	± 6	1.08
Radial Blanket	96.680	25	± 5	0.78	9	± 5	2.29

TABLE XII. Results of the U-6 (^{235}U) Radial Reactivity Traverse

Zone	Position, cm	Reference Core Measured Worth, Ih/kg	C/E	H240-Zoned Core Measured Worth, Ih/kg	C/E
Control Rod	2.764	70.91 ± 0.06		71.56 ± 0.07	1.10
Inner Core	8.288	77.67 ± 0.09	1.12	79.17 ± 0.10	1.11
	13.813	80.63 ± 0.11	1.13	81.48 ± 0.09	1.14
	19.337	80.91 ± 0.09	1.14	81.66 ± 0.07	1.15
	24.862	78.88 ± 0.08	1.16	80.33 ± 0.09	1.17
	30.386	76.61 ± 0.10	1.16	77.35 ± 0.09	1.18
	35.911	72.96 ± 0.11	1.18	73.78 ± 0.11	1.19
	41.435	68.48 ± 0.11	1.19	68.52 ± 0.10	1.21
	46.960	63.06 ± 0.11	1.20	62.52 ± 0.09	1.22
	52.484	56.63 ± 0.09	1.20	56.28 ± 0.09	1.22
↓	58.009	49.10 ± 0.12	1.21	48.26 ± 0.12	1.22
Control Rod	63.533	39.11 ± 0.10	1.20	37.79 ± 0.12	1.23
Control Rod	69.058	33.05 ± 0.08	1.19	32.32 ± 0.10	1.21
Outer Core	74.582	30.10 ± 0.07	1.23	29.34 ± 0.09	1.25
	80.107	26.60 ± 0.10	1.22	26.11 ± 0.08	1.25
↓	85.631	22.10 ± 0.12	1.22	21.87 ± 0.11	1.23
Radial Blanket	91.156	17.76 ± 0.09	1.18	17.73 ± 0.10	1.19
	96.680	12.72 ± 0.12	1.20	12.54 ± 0.08	1.21
	102.205	8.84 ± 0.23	1.12	8.71 ± 0.26	1.12
	107.729	5.55 ± 0.23	1.06	5.59 ± 0.23	1.03
	113.254	3.35 ± 0.22	0.97	3.41 ± 0.25	0.95
	118.778	2.04 ± 0.22	0.83	1.33 ± 0.24	1.36
↓	124.303	1.14 ± 0.22	0.76	0.51 ± 0.25	2.07
Reflector	129.827	0.43 ± 0.23	0.96	-0.01 ± 0.24	
Reflector	135.352	0.39 ± 0.22		0.15 ± 0.24	
Matrix	140.876	0.12 ± 0.23		-0.06 ± 0.25	
Matrix	146.401	0.00 ± 0.04		0.00 ± 0.04	

TABLE XIII. Results of the DU-6 (^{238}U) Radial Reactivity Traverse

Zone	Position, cm	Reference Core Measured Worth, Ih/kg	C/E	H240-Zoned Core Measured Worth, Ih/kg	C/E
Control Rod	2.764	-3.67 ± 0.04		-3.78 ± 0.04	0.79
Inner Core	8.288	-4.28 ± 0.07	1.15	-4.11 ± 0.06	1.22
	13.813	-5.07 ± 0.06	1.27	-5.33 ± 0.07	1.24
	19.337	-5.40 ± 0.06	1.31	-5.75 ± 0.07	1.26
	24.862	-5.76 ± 0.06	1.25	-5.54 ± 0.06	1.34
	30.386	-5.57 ± 0.06	1.27	-5.38 ± 0.06	1.36
	35.911	-4.91 ± 0.07	1.39	-5.20 ± 0.06	1.34
	41.435	-4.85 ± 0.06	1.30	-4.82 ± 0.06	1.33
	46.960	-4.01 ± 0.07	1.40	-3.98 ± 0.06	1.42
	52.484	-3.17 ± 0.06	1.42	-2.88 ± 0.06	1.56
∨	58.009	-1.86 ± 0.07	1.54	-1.66 ± 0.06	1.71
Control Rod	63.533	-1.59 ± 0.06	0.89	-1.69 ± 0.06	0.85
Control Rod	69.058	-1.77 ± 0.06	0.90	-1.78 ± 0.06	0.92
Outer Core	74.582	-1.84 ± 0.06	1.21	-2.00 ± 0.06	1.15
	80.107	-1.60 ± 0.06	1.33	-1.62 ± 0.06	1.35
↓	85.631	-0.95 ± 0.06	1.63	-1.06 ± 0.06	1.51
	91.156	-0.21 ± 0.06		-0.15 ± 0.06	
Radial Blanket	96.680	0.19 ± 0.06	1.12	0.31 ± 0.06	0.67
	102.205	0.13 ± 0.15	0.46	0.64 ± 0.16	
	107.729	-0.05 ± 0.15	0.41	0.47 ± 0.16	
	113.254	-0.23 ± 0.15		0.42 ± 0.16	
	118.778	0.12 ± 0.15		-0.18 ± 0.16	
∨	124.303	0.30 ± 0.15		-0.26 ± 0.17	
Reflector	129.827	0.04 ± 0.15		-0.12 ± 0.16	
Reflector	135.352	0.09 ± 0.15		-0.08 ± 0.16	
Matrix	140.876	-0.38 ± 0.15		-0.17 ± 0.16	
Matrix	146.401	0.00 ± 0.03		0.00 ± 0.03	

TABLE XIV. Results of the SS-1 (Stainless Steel) Radial Reactivity Traverse

Zone	Position, cm	Reference Core Measured Worth, Ih/kg	C/E	H240-Zoned Core Measured Worth, Ih/kg	C/E
Control Rod	2.764	−3.32 ± 0.04		−3.30 ± 0.05	0.72
Inner Core	8.288	−2.61 ± 0.08	0.98	−2.25 ± 0.08	1.22
	13.813	−3.31 ± 0.08	1.06	−3.27 ± 0.09	1.13
	19.337	−3.12 ± 0.08	1.21	−3.78 ± 0.09	1.06
	24.862	−3.57 ± 0.08	1.04	−3.48 ± 0.09	1.14
	30.386	−3.29 ± 0.08	1.08	−3.09 ± 0.09	1.23
	35.911	−2.64 ± 0.10	1.27	−2.91 ± 0.08	1.23
	41.435	−2.79 ± 0.08	1.12	−2.39 ± 0.09	1.38
	46.960	−2.22 ± 0.08	1.24	−1.98 ± 0.09	1.43
	52.484	−1.37 ± 0.08	1.49	−0.86 ± 0.08	2.40
	58.009	−0.47 ± 0.09	1.96	−0.04 ± 0.08	
Control Rod	63.533	−1.04 ± 0.09	0.77	−0.90 ± 0.09	0.86
Control Rod	69.058	−1.94 ± 0.09	0.79	−1.70 ± 0.08	0.98
Outer Core	74.582	−1.70 ± 0.07	0.98	−1.79 ± 0.08	1.43
	80.107	−1.20 ± 0.09	1.05	−0.94 ± 0.08	2.11
	85.631	−0.19 ± 0.08	2.53	−0.14 ± 0.09	
	91.156	0.60 ± 0.07	0.52	0.82 ± 0.08	0.38
Radial Blanket	96.680	1.09 ± 0.08	0.61	1.47 ± 0.07	0.47
	102.205	0.62 ± 0.20	0.73	1.06 ± 0.20	0.43
	107.729	0.60 ± 0.19	0.39	0.81 ± 0.21	
	113.254	0.12 ± 0.20	0.94	0.52 ± 0.21	
	118.778	−0.31 ± 0.19		0.26 ± 0.21	
	124.303	0.17 ± 0.20		0.21 ± 0.21	
Reflector	129.827	0.17 ± 0.20		−0.15 ± 0.21	
Reflector	135.352	−0.01 ± 0.19		0.04 ± 0.20	
Matrix	140.876	−0.46 ± 0.20		−0.01 ± 0.18	
Matrix	146.401	0.00 ± 0.04		0.00 ± 0.04	

XV. Results of the B-1 (^{10}B) Radial Reactivity Traverse

Zone	Position, cm	Reference Core Measured Worth, Ih/kg			C/E	H240-Zoned Core Measured Worth, Ih/kg			C/E
Control Rod	2.764	−696	±	1		−709	±	1	0.86
Inner Core	8.288	−971	±	3	1.03	−996	±	1	1.01
	13.813	−1206	±	1	1.03	−1219	±	2	1.04
	19.337	−1313	±	1	1.03	−1324	±	1	1.04
	24.862	−1347	±	1	1.04	−1346	±	1	1.05
	30.386	−1329	±	1	1.04	−1321	±	1	1.06
	35.911	−1263	±	1	1.06	−1249	±	1	1.08
	41.435	−1166	±	1	1.07	−1147	±	1	1.09
	46.960	−1035	±	1	1.08	−1007	±	1	1.11
	52.484	−850	±	1	1.10	−817	±	2	1.14
	58.009	−613	±	3	1.12	−576	±	1	1.17
Control Rod	63.533	−384	±	3	0.97	−359	±	1	1.01
Control Rod	69.058	−331	±	1	0.95	−316	±	1	0.97
Outer Core	74.582	−384	±	1	1.10	−375	±	1	1.12
	80.107	−384	±	1	1.14	−376	±	1	1.16
	85.631	−331	±	1	1.13	−319	±	1	1.17
	91.156	−240	±	1	1.14	−235	±	1	1.17
Radial Blanket	96.680	−144	±	1	1.12	−137	±	1	1.18
	102.205	−79	±	3	1.04	−79	±	3	1.05
	107.729	−38	±	3	1.05	−36	±	3	1.11
	113.254	−21	±	3	0.83	−15	±	3	1.15
	118.778	−13	±	3	0.59	−7	±	3	0.69
	124.303	−7	±	3	0.52	−5	±	3	
Reflector	129.827	0	±	3	2.60	−8	±	3	0.44
Reflector	135.352	1	±	3		−6	±	3	
Matrix	140.876	−7	±	3		−3	±	3	
Matrix	146.401	0	±	3					
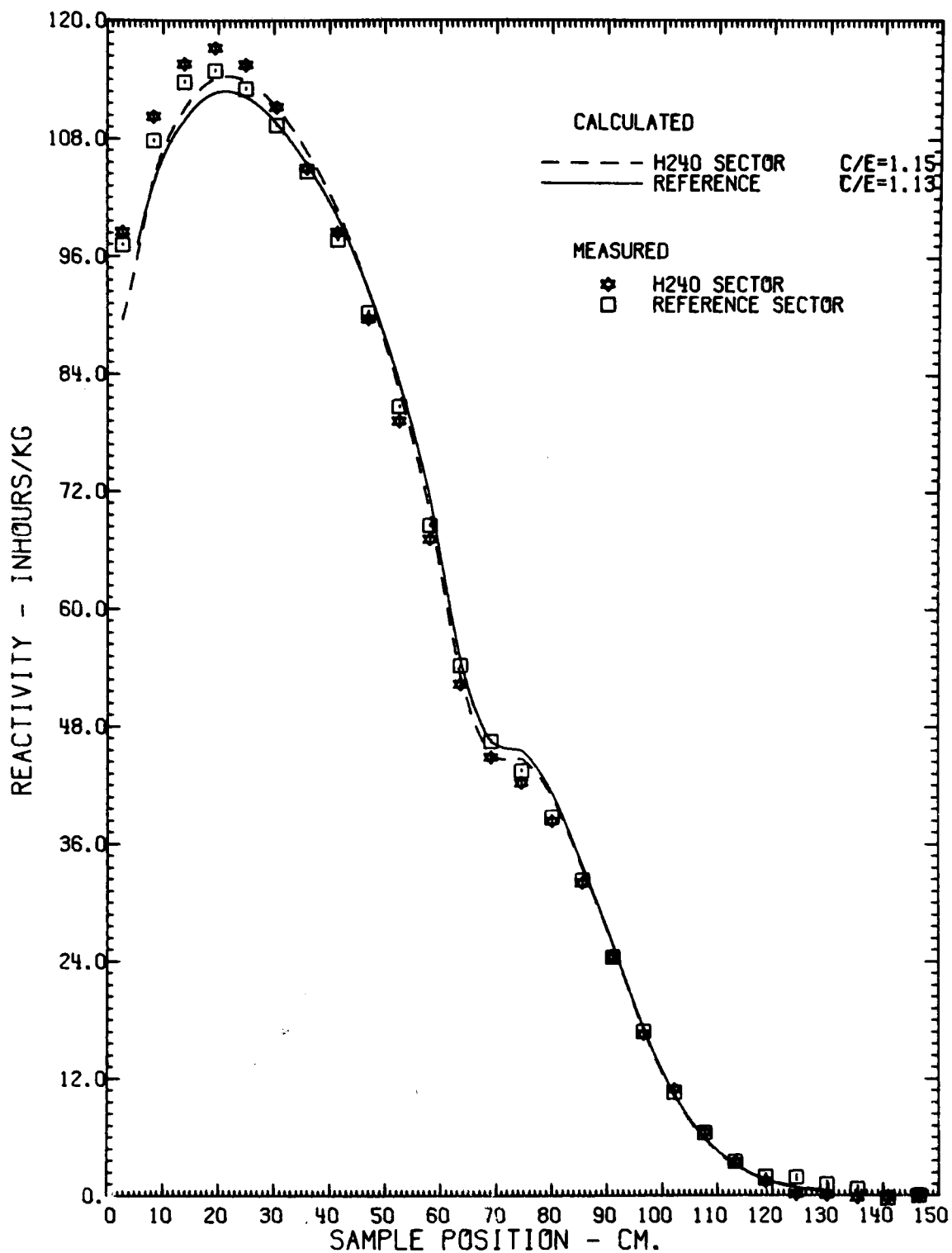
Fig. 7. The Pu-30 (^{239}Pu) Radial Reactivity Traverses.
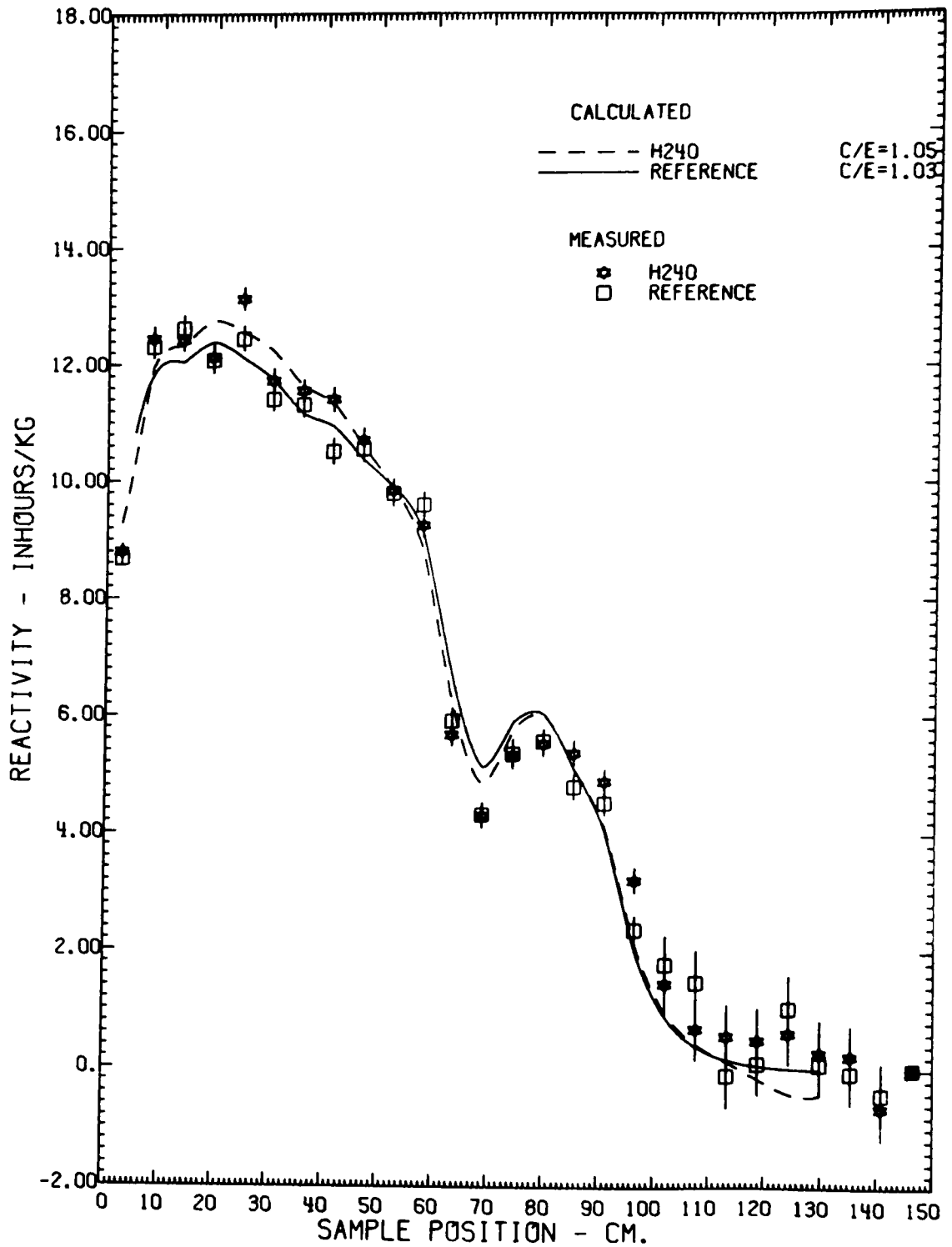
Fig. 8. The P240-R (^{240}Pu) Radial Reactivity Traverses.
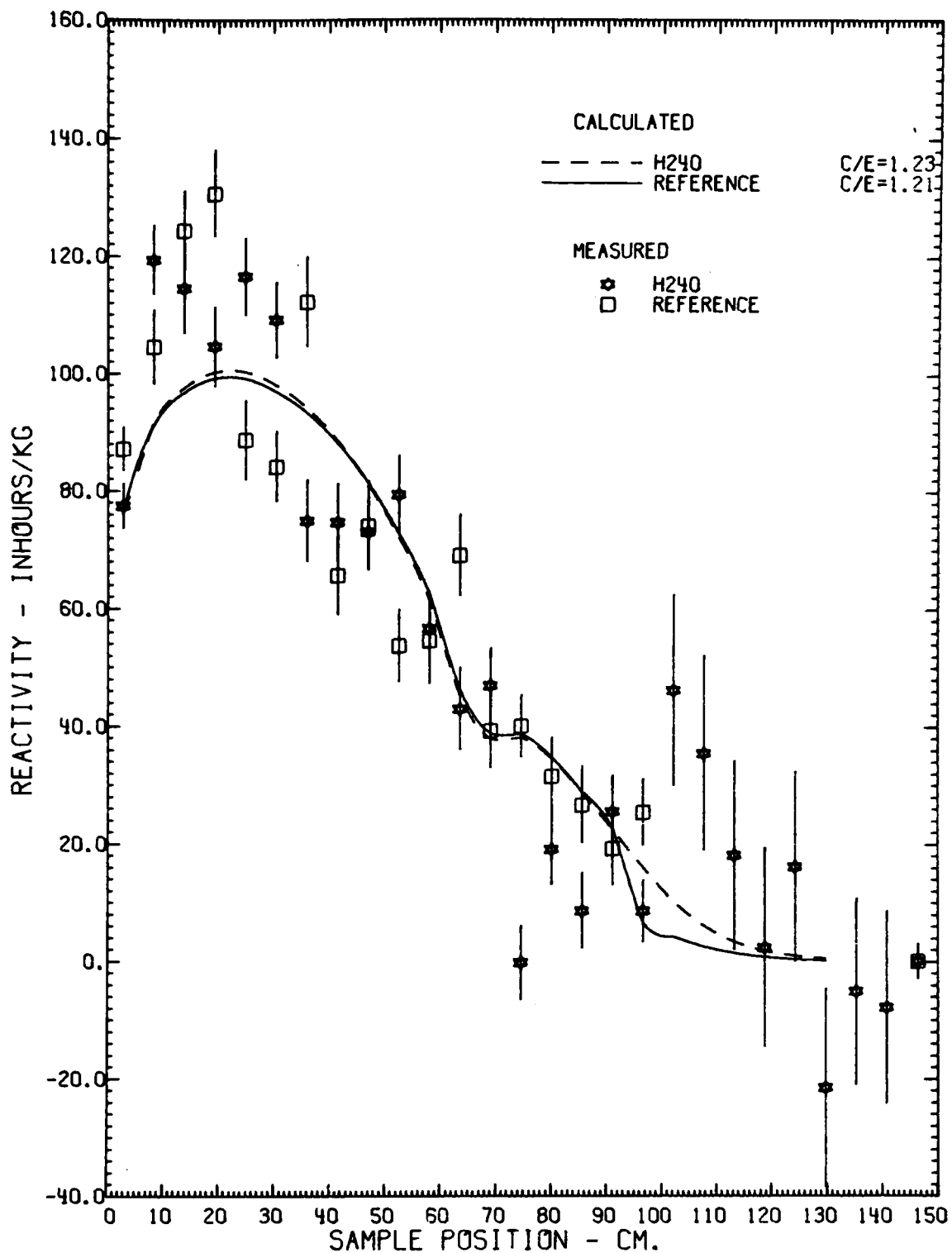
Fig. 9. The Pu-50 (^{241}Pu) Radial Reactivity Traverses.
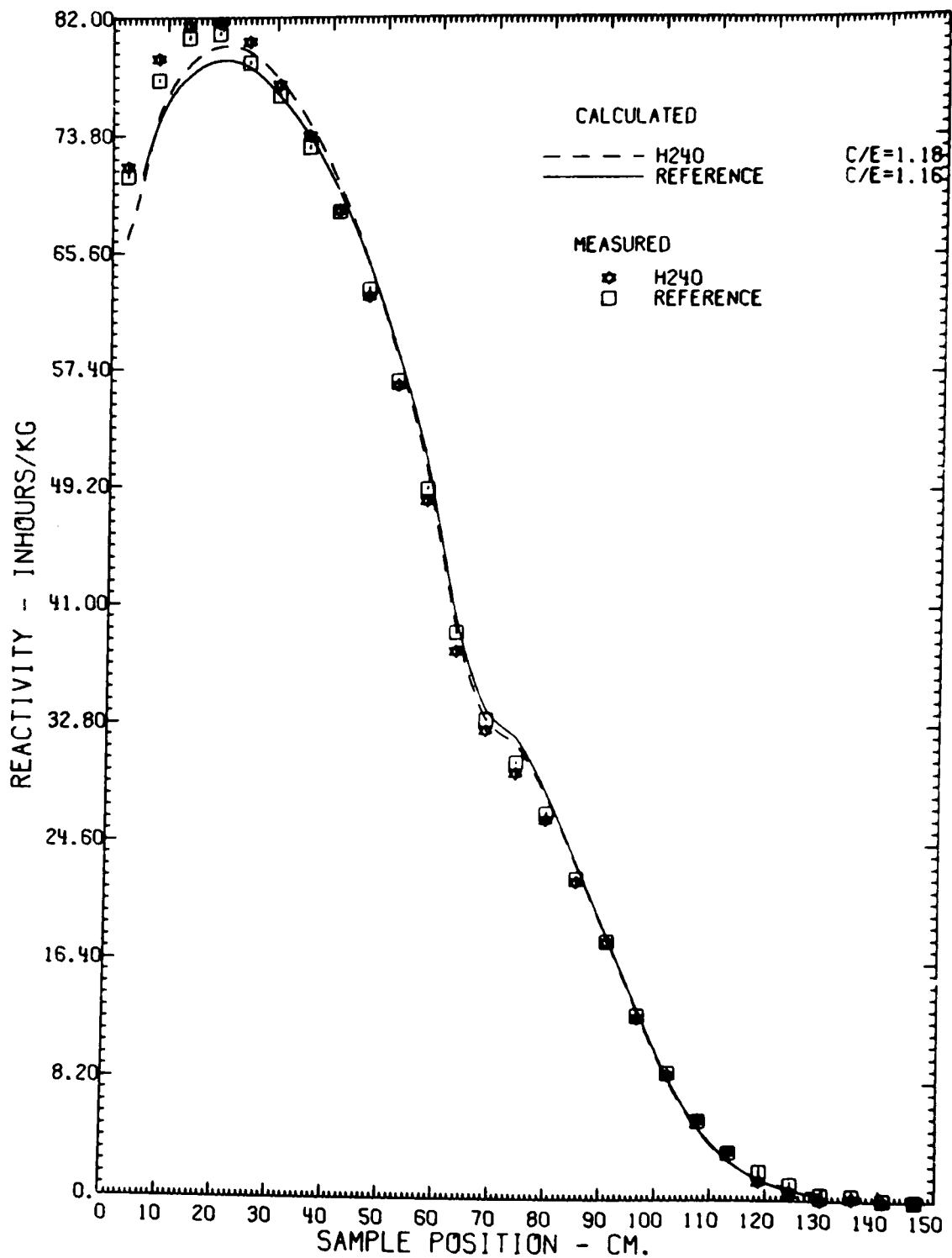
Fig. 10. The U-6 (^{235}U) Radial Reactivity Traverses.
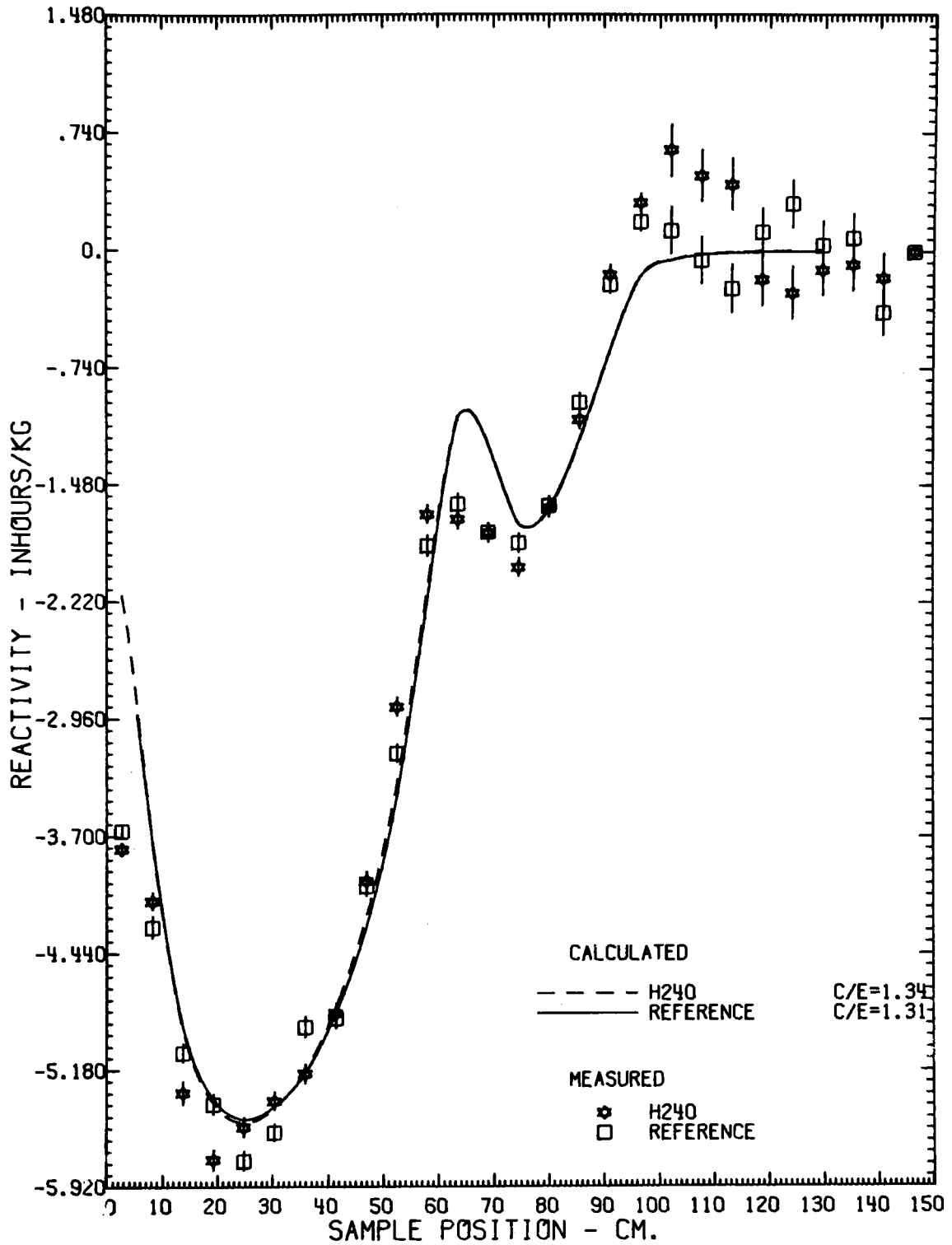
Fig. 11. The DU-6 (^{238}U) Radial Reactivity Traverses.
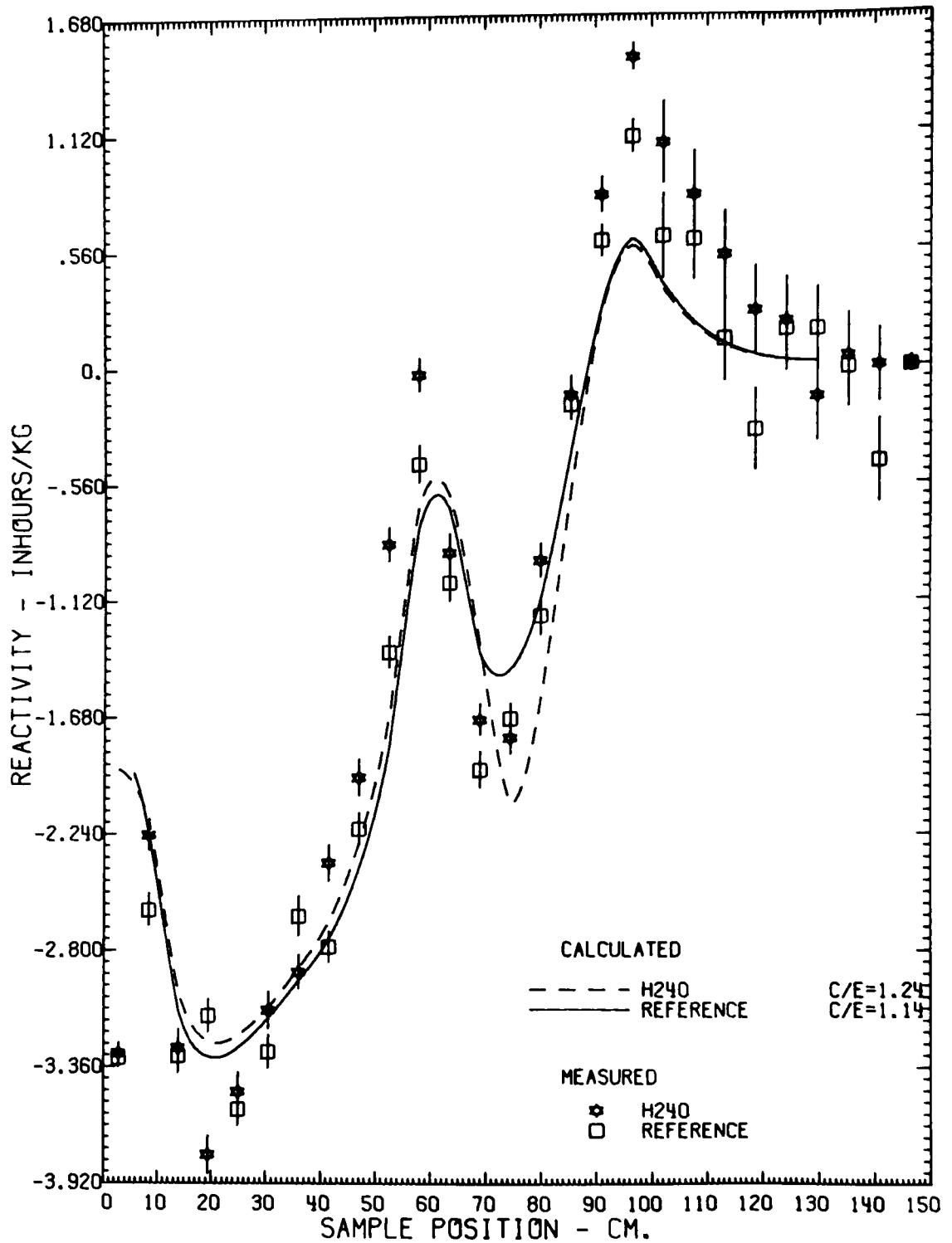
Fig. 12. The SS-1 (Stainless Steel) Radial Reactivity Traverses.
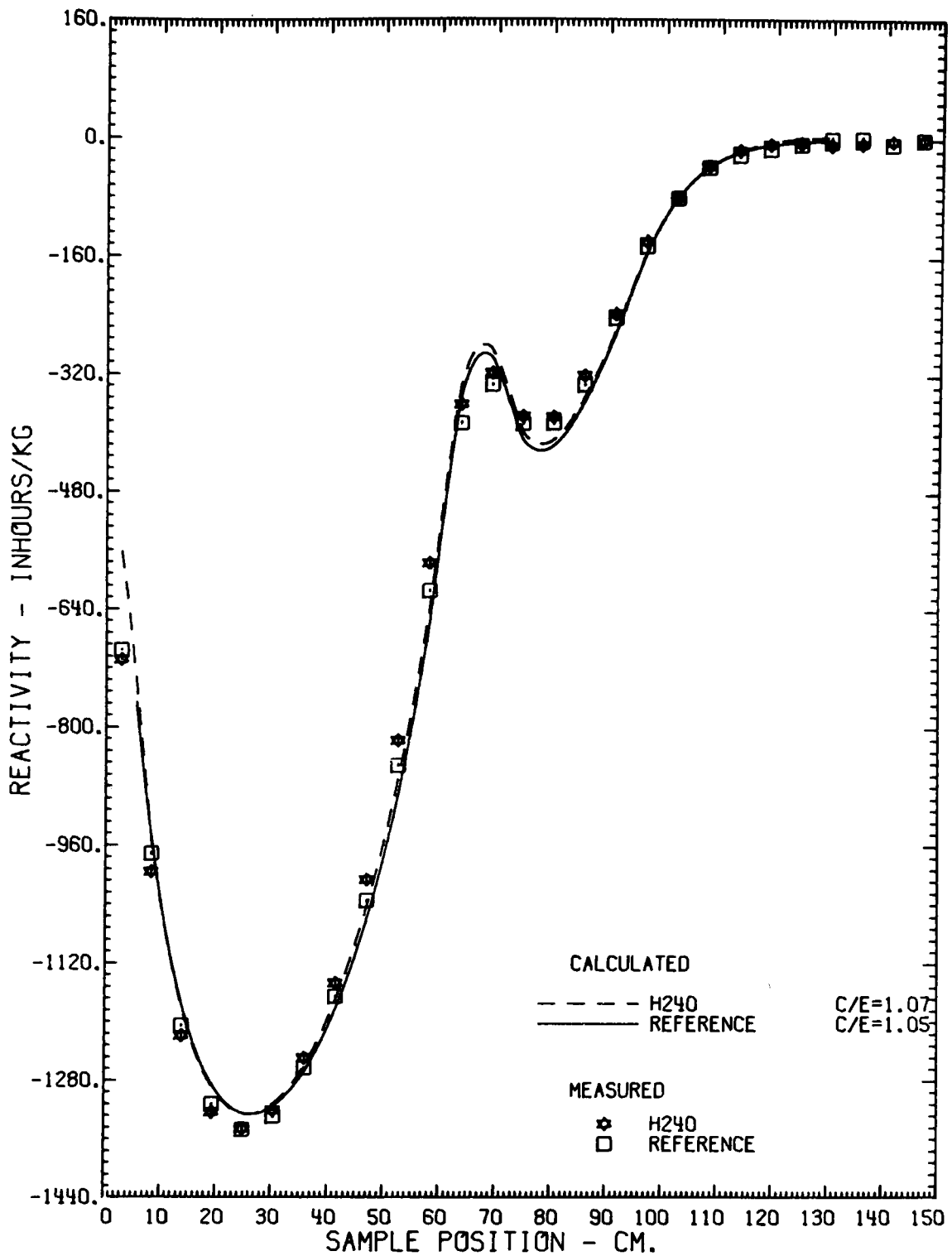
Fig. 13.   The B-1 (^{10}B) Radial Reactivity Traverses.
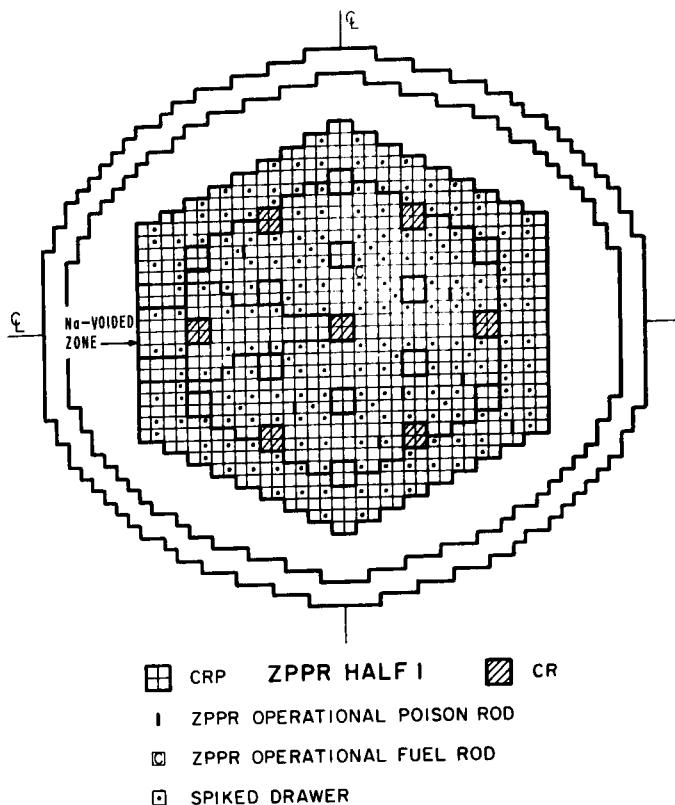
Fig. 14. The Sodium Void Zone in the High ^{240}Pu Experiment.

front 12 in. of the drawers. Previous experience on other Benchmark critical assemblies has shown that voiding ±12 in. axially yields the maximum sodium-void reactivity throughout most of the core region. The second step was to void the full core height, i.e., ±18 in.

The actual measurement technique involved determining the excess reactivity (k_{ex}) for each configuration. To accomplish this, a poison shim rod was calibrated in the reference (unvoided) configuration. Then, for each configuration the rod position was recorded for a fixed power level. This level corresponded to a countrate of 50,000/sec on the 10^{-7} scale of PICO No. 1, which is an external ionization chamber with a voltage-to-frequency converter. The average temperature as determined from distributed thermocouples was also recorded. Finally, the readings of the gap width indicators were recorded. The excess reactivity for the voided configurations, as determined by the calibrated shim rod, was corrected to the same temperature, gap width, and ^{241}Pu content as the reference configuration. The worth of each voiding step was determined by subtracting k_{ex} for the voided configuration from the reference k_{ex}.

It was recognized prior to the experiment that the measured worth, i.e., Δk_{ex}, would be quite small. This is due to a change of sign in the sodium worth in the outer core. Furthermore, the zone was small. Because of the anticipated small Δk_{ex}, an alternate measurement technique was tried. The object was to bypass the uncertainty in the measurement caused by temperature, ^{241}Pu decay, and gap closure corrections. The limitation in the alternate

method was that the sodium void worth in only a single drawer could be mea-
sured. For this measurement, one drawer within the zone was connected to a
control rod drive mechanism. Then, during a reactor run, the drawer (matrix
position 136-21) was oscillated and the "out" to "in" reactivity change was
determined from inverse kinetics analysis of the PICO signal. The worth of
the drawer in the voided state was subtracted from the worth in the reference
state to determine the void worth. The drawer in this experiment was located
in matrix position 136-21.

Results of the two types of sodium-void measurements are presented in
Tables XVI and XVII. The results for the 4 x 4 drawer zone show a definite

TABLE XVI. Results of Outer-Core Sodium-Void Reactivity Measurements

Configuration	Sodium Mass, kg	Reference Core Reactivity Coefficient, Ih/kg			H240-Zoned Core Reactivity Coefficient, Ih/kg		
		Measured[a]	Calculated	C-E	Measured[a]	Calculated	C-E
±12 in. void	10.297	0.63 ± 0.08	0.49	-0.14	1.07 ± 0.06	0.65	-0.42
±18 in. void	15.453	0.08 ± 0.05	0.02	-0.06	0.39 ± 0.04	0.15	-0.24

[a]Statistical uncertainty on control rod calibration only.

TABLE XVII. Results of Single-Drawer Oscillator Measurement of Sodium-Void Reactivity

Configuration	Reactivity Relative to Unvoided Condition, Ih		H240-Normal Reactivity Difference, Ih
	Reference Core	H240 Zone	
Oscillator voided 12 in.[b] axially	-0.233 ± 0.007[a]	-0.123 ± 0.007	+0.110 ± 0.010
Oscillator voided 12 in. in 4 x 4 drawer zone voided ±12 in. axially	+0.294 ± 0.007	+0.544 ± 0.007	+0.250 ± 0.010
Oscillator voided 18 in.[c] in 4 x 4 drawer zone voided ±18 in. axially	-0.172 ± 0.007	+0.050 ± 0.007	+0.222 ± 0.010

[a]Uncertainties are statistical only.

[b]0.404 kg Na.

[c]0.606 kg Na.

increase in worth in the H240 environment. This is in contrast to the central
worth measurements in ZPR-6 assembly 7 [1]. There, the ratio of central
sodium-void worths, when corrected for the difference in perturbation denomi-
nators, was very nearly 1.0. The measurement in ZPPR assembly 4, however, is
much more difficult to interpret. Since the sodium void zone encompassed the
region where the sodium coefficient changes sign, only slight changes in the
gradient can cause large percentage changes in the results. It is therefore
essentially impossible to separate the H240 spectral effects from effects
caused by changes in the gradient. The same argument applies to the single
drawer measurements. In Table XVII we note that in both cases there is a
relatively large change for the 12 in. voided drawer from the reference to the
4 x 4 voided zone. We suspect that most of this change must be due to a change
in the flux gradient.

One possible means of removing most of the effect of the radial gradient
is to compare the differences between the 12 in. and the 18 in. void results.

For this difference, the H240/normal ratio is 1.23 for the 4 x 4 drawer zone and 1.06 for the single drawer oscillator.

FOP, constant buckling, calculations in xy geometry were done in support of these measurements. Results of the calculations are also presented in Table XVI. Because the signal is so close to zero, we have reported C-E values rather than the usual C/E ratios. The C-E values were within 2σ for the reference core, but were considerably outside statistics for the H240-zoned core. However, since the total signal is so small, the magnitude of the difference between the measured and calculated results is almost insignificant.

C. ^{238}U Doppler Coefficient Measurements

The Doppler coefficient of a 1 kg sample of natural UO_2 was measured in both the normal and the H240-zoned cores [19,20]. The measurements were centered in the outer core in a position such that an equilibrium spectrum with the high-^{240}Pu fuel could be achieved. (Refer to Fig. 1, matrix position 136-21). Comparative measurements were made at nominal temperatures of 650°K, 800°K and 950°K.

The measurement technique [21,22] was to oscillate the hot sample in and out of the cold reactor. Data from the external PICO detectors were recorded by the SEL-840 computer and analyzed by inverse kinetics. The worth of the Doppler sample was measured against the worth of a dummy capsule, much as was done with the small reactivity samples. (See p. 18, this report.) A more complete description of the experimental and calculational procedures employed for ZPPR Doppler measurements is presented in Ref. 23.

A comparison between results in the normal core and the H240-zoned core is presented in Table XVIII. The Doppler effect is seen to be reduced by about 10% in the H240 case. This is attributed to hardening of the low energy spectrum with the high-^{240}Pu fuel. The 10% value corresponds favorably to the 12% value measured in the central H240 zone of ZPR-6, assembly 7 [1].

Comparative calculations are not available at this time. The Doppler effect in similar ZPPR cores has been calculated with a C/E close to unity.

D.   Control Rod Substitution Measurements

Measuring the effect of the high-^{240}Pu fuel on control rod worths was made difficult by the fact that the only control rod position within the H240 sector was filled with an inserted rod. The experimental technique, therefore, involved replacing the reference control rod (CR-13 in Fig. 1) with a rod more heavily loaded with ^{10}B. To accomplish this end the reference design N-1 control rod was replaced by a design M control rod. The design N-1 rod simulates the initial core rods for the CRBR, while the design M rod simulates the equilibrium core rods for the CRBR. B_4C masses for the design N-1 rod and the design M rod are 8.71 kg and 15.90 kg, respectively. The appropriate number densities are presented in Table II.

In both configurations the rod substitution reactivity was measured by two methods: polarity coherence (noise) and subcritical multiplication [24,25].

TABLE XVIII. Comparison of $^{238}UO_2$ Doppler Coefficient Measurements

Sample Temperature, $^{\circ}K$	Doppler Reactivity Coefficient, $Ih/kg\ ^{238}U$		H240/Reference
	H240 Zoned Core	Reference Core	
650	-0.0491 ± 0.0016	-0.0535 ± 0.0011	0.918
800	-0.0598 ± 0.0015	-0.0668 ± 0.0011	0.895
950	-0.0717 ± 0.0015	-0.0802 ± 0.0011	0.894

These methods were calibrated in the reference state by a rod drop. Results of individual measurements are presented and compared in Table XIX. Results for individual detectors are not corrected for efficiency changes and effective source changes [26]. However, this should not affect the comparison between the two results for the same detector. Furthermore, previous experience has shown that only minor corrections are required for effective source and detector efficiency when the change in reactivity is small.

A total of five detectors was employed in the subcritical source multiplication measurement. These were: (1) a BF_3 proportional counter in the plenum behind Half 1, (2) a BF_3 proportional counter on the wall of the reactor cell behind Half 2, (3) the two PICO BF_3 ionization chambers located radially above the reactor and (4) a ^{235}U fission chamber at the radial blanket-outer core interface in matrix position 234-54. The ^6Li polarity-coherence detectors were located in matrix positions 124-45 and 125-46.

K-difference calculations of the rod substitution worths were made. The calculations employed 2D (xy) diffusion theory in 28 energy groups. Results of these calculations appear in Table XIX along with results of the measurements. Infinite dilute boron cross sections were used. There are several deficiencies in these calculations. Because of the way the boron carbide is lumped within the CR drawers, self-shielding factors should be applied to the boron cross sections. There are transport effects in and around the control rod. Studies underway show a definite mesh spacing sensitivity in control rod calculations. Yet C/E ratios near unity are routinely obtained for control rod calculations of this type. There is evidence [27] that a fortuitous cancellation of errors is partly responsible for this gratifying result. However, as with the deficiencies in the experimental results, the calculational results are acceptable for comparative purposes.

The average measured change in the control rod worth was -1.5 ± 1.0%. The calculated change was -0.5%, adequately within the bounds of the experiment. Significantly, there was little difference in the two cases, and that small difference was reflected in the calculations. Because of the small absolute difference, it is impossible to tell whether the decrease in worth resulted from a spectral shift due to the H240 fuel, or from a slight change in flux gradients in the vicinity of the rod.

V. REACTION RATES: MEASUREMENT AND CALCULATION

Three reaction rate measurement techniques were employed in the ZPPR assembly 4, phase 2 cores. These were (1) measurement of the radial Pu-fission distribution with a remotely traversable fission chamber [4], (2) TLD measurement of gamma-ray heating in stainless steel [28], and (3) measurement of the $^{239}Pu(n,f)$, $^{235}U(n,f)$, $^{238}U(n,\gamma)$, and $^{238}U(n,f)$ reaction rates with foils [29]. Because of the complicated nature of the gamma-ray heating experiments and calculations, we shall leave them to a separate report. The Pu fission counter traverse contributed significantly to the determination of the final H240 sector configuration. The foil measurements comprised the most extensive set of comparative measurements in the H240 experiment.

TABLE XIX. Results of Control Rod Substitution Measurements

Method	Substition Worth, $ H240 Zone	Reference	H240/Ref
Polarity Coherence	-0.764 ± 0.011	-0.769 ± 0.006	0.993
Fission Chamber in Radial Blanket	-0.747 ± 0.018	-0.767 ± 0.008	0.974
Axial BF_3 Proportional Counters	-0.780 ± 0.011	-0.784 ± 0.008	0.995
Radial BF_3 Ionization Chambers	-0.760 ± 0.009	-0.779 ± 0.008	0.975
Average Measured	-0.763 ± 0.024	-0.775 ± 0.014	0.985
Calculated	-0.776	-0.780	0.995
Average C/E	1.017	1.006	1.010

A. The ^{239}Pu Fission Counter Traverse

^{239}Pu fission counter traverses were made in the slot at the reactor mid-plane for the purpose of defining the H240 zone. The fuel spiking pattern was adjusted to make the shape of the radial ^{239}Pu fission distribution the same in both the normal core and the H240 sector.

The fission counter was moved across the core with the same radial traverse mechanism that was used for the small reactivity samples. A description of the counter foil is found in Table XX. The countrate at each position was normalized to that of a stationary fission chamber on the opposite side of the reactor. The measurements were made at about 0.20$ subcritical.

Results of these traverses are presented in Fig. 3 and Table XXI. Both the measured and calculated fission rates show close agreement between the H240 sector and the normal core. The exception is in the narrow end of the sector near the central control rod. Since no spikes were in this region, fine tuning of the fission rate was not possible. Nevertheless, the fission rates agreed within 1% throughout the sector and the radial blanket. In both cases the C/E ratios were near unity for most of the inner core. Some difference is noted around the inserted control rods. Both C/E ratios average 1.04 in the outer core. (Comparable C/E ratios for the foils are closer to unity.) In the blanket the C/E falls off monotonically with increasing radius, but no difference is noted between the H240 and the reference case.

The foregoing discussion reveals that not only was the fission rate shape matched when the H240 zone was loaded, but also the pointwise fission rates were matched in an absolute sense. From the relative C/E values it is obvious that there was no calculational disadvantage in using the fuel with the larger concentration of the higher plutonium isotopes.

B. The Foil Measurements and Calculations

Foils of ^{239}Pu, ^{238}U, and ^{235}U were used to measure reaction rates in core and blanket regions. The neutron capture rate in ^{238}U as well as the fission rates of all three isotopes were measured. The foils were placed in the reactor and irradiated for several hundred watt-hours. They were then removed from the reactor and the appropriate fission products or activation products were counted. Since the efficiency of the counting system is known and the total integrated power history was recorded, absolute reaction rates are reported for the foils.

Foils were placed within the drawers in standard steel shims which could hold all three types of foils in position simultaneously. The foils were loaded into the unit cells (refer to Fig. 2) according to the following prescription [29]: (1) Within the inner core, foils were adjacent to the central fuel plate on the side toward the vertical centerline of the core. (2) Double column outer core fuel drawers had the foils located on the fuel plate surface closest to the core center. (3) Single column outer core drawers followed the same convention as inner core drawers. (4) In the radial blanket, the foils were located in the center of the ½-in. U_3O_8 column closest to the vertical centerline. All foil measurements were done in Half 1. In the normal config-

TABLE XX. Description of the ^{239}Pu Traverse Counter Fission Foil

Mass, µg	Composition	
107.7 ± 1.1	^{239}Pu	94.429 ± 0.018%
	^{240}Pu	5.283 ± 0.014%
	^{241}Pu	0.274 ± 0.012%
	^{242}Pu	0.013 ± 0.001%

TABLE XXI. Results of ^{239}Pu Fission Counter Traverse in the Two Reference Cores

Matrix Position	Zone	Normalized[a] Reaction Rate						H240/Ref
		Reference			H240 Zone			
		Exp[b]	Calc	C/E	Exp[b]	Calc	C/E	
137-36	Control Rod	1157.5	1079.3	0.93	1173.9	1091.0	0.93	1.01
137-35	Inner Core	1303.4	1306.1	1.00	1319.5	1317.0	1.00	1.01
137-34		1410.5	1405.3	1.00	1422.4	1416.7	1.00	1.01
137-33		1454.1	1450.7	1.00	1472.4	1462.2	0.99	1.01
137-32		1468.6	1466.6	1.00	1471.5	1477.5	1.00	1.00
137-31		1459.5	1458.5	1.00	1464.4	1467.4	1.00	1.00
137-30		1428.8	1433.6	1.00	1429.8	1439.7	1.01	1.00
137-29		1369.6	1385.1	1.01	1374.6	1387.8	1.01	1.00
137-28		1297.7	1318.1	1.02	1288.2	1316.4	1.02	0.99
137-27		1192.2	1221.6	1.02	1183.1	1216.0	1.03	0.99
137-26		1046.7	1087.1	1.04	1040.0	1079.1	1.04	0.99
137-25	Control Rod	861.8	847.5	0.98	852.8	838.7	0.98	0.99
137-24	Control Rod	788.5	779.3	0.99	782.1	771.4	0.99	0.99
137-23	Outer Core	809.5	846.7	1.05	804.2	841.5	1.05	0.99
137-22		793.1	824.2	1.04	788.6	821.1	1.04	0.99
137-21		733.1	759.5	1.04	725.1	757.0	1.04	0.99
137-20		650.8	664.4	1.02	645.2	661.9	1.03	0.99
137-19	Radial Blanket	547.0	563.8	1.03	546.4	561./	1.03	1.00
137-18		454.0	449.7	0.99	449.0	447.9	1.00	0.99
137-17		360.8	348.1	0.96	358.4	346.8	0.97	0.99
137-16		288.1	263.5	0.91	285.8	262.3	0.92	0.99
137-15		235.8	197.1	0.84		196.1		
137-14		205.1	148.9	0.73	202.3	148.1	0.73	0.99
137-13	Reflector		120.2			119.6		
137-12		148.2	57.1	0.39	146.9	56.7	0.39	0.99

[a]Normalized to ^{239}Pu fission chamber on opposite side of core.

[b]Statistical uncertainty = 1%.

uration, just the upper left-hand quadrant was used. The upper two quadrants were used in the H240-zoned configuration. The distance from the interface for the ^{239}Pu, ^{238}U, and ^{235}U foils was 90.805 mm, 76.92 mm and 63.119 mm, respectively.

The end product of the foil data processing contains all the foil location information and the absolute reaction rate data. These data are processed by a utility code which translates the matrix locations and intracell positions to appropriate coordinates for the corresponding neutronics calculation. A second card set, generated by this utility code, is in turn input to the TOPSY code. TOPSY takes the fluxes from the calculation of reference critical configuration and uses Lagrangian interpolation to generate fluxes at the measurement points. Cell-averaged cross sections for the appropriate region are then summed with the point fluxes to obtain calculated reaction rates. Calculated-to-experimental ratios are automatically computed for each point and each reaction.

The experimental values require cell averaging for direct comparison to the calculations. Furthermore, the TOPSY output requires normalization such that the experiments and calculations correspond to the same reactor power. This normalization was achieved by requiring that the average C/E for plutonium fission be 1.00 for the inner core. This same normalization factor was used for each reaction rate. Separate normalizations were required for the H240 and the normal case since the power histories differed. The matter of cell-averaging factors for the experimental reaction rates is less crucial in the H240/normal comparison. Since our principal interest is in the changes in reaction rates from the normal to the H240 case, cell-averaging factors are of little value so long as we can assume that they are the same for both the H240 and the normal case. Because the cell-averaging factors are effectively 1.0 for ^{239}Pu and ^{235}U, small changes in fuel composition certainly do not affect these reactions. The significant cell-averaging factors are for ^{238}U capture and fission. There may be slight changes in these cell-averaging factors due to the 10% reduction in ^{238}U content in the H240 fuel plates.

For the purposes of this study we have applied the cell-averaging factors in Table XXII to both the H240 and the normal measurements. We have used values of 1.0 for ^{235}U and ^{238}U fission. The ^{238}U fission rate should be adjusted by a cell-averaging factor several percent different from unity, but those numbers were not available for this study. To be strictly correct, different cell-averaging values for ^{238}U capture should be used near spikes, CRPs, CRs, double-column drawers and boundaries. Again, since we are interested in comparative measurements, we have applied only region-averaged values.

The extensiveness of these measurements makes a coherent evaluation of the results challenging if not impossible. Our attempt at coherence in this task is to organize the discussion into four sections, considering all four types of reactions in each section. First, we consider region-averaged C/E ratios for the H240 and normal configurations. Next we present comparative maps of absolute reaction rates. Comparable C/E maps follow. Finally, we compare reaction rates on the H240 side and the normal side of the H240-zoned configuration.

TABLE XXII. Cell-Averaging Factors Applied to the Foil Measurements

Reaction	Region	Cell-Averaging Factor
$^{239}Pu(n,f)$	Inner Core	0.995
$^{239}Pu(n,f)$	Outer Core	0.995
$^{238}U(n,\gamma)$	Inner Core	0.9129
$^{238}U(n,\gamma)$	Outer Core	0.8965
$^{238}U(n,\gamma)$	Radial Blanket	0.9645

The region-averaged C/E ratios are compared for the normal and the H240 case in Table XXIII. The normalization is such that C/E is 1.0 for inner-core plutonium fission. One striking feature in the table is that the C/E ratios in the H240 core are systematically higher than the corresponding ratios in the normal core. The difference is generally 0.5 - 2.0%. If we normalize the reference case over just the same spatial locations that were used in the H240 case, the difference in C/E ratios decreases by almost 1%. One standard deviation of C/E is about the same in both cases. The 2% difference in the c^{28}/f^{49} values is possibly due to a real difference in the cell-averaging factors for ^{238}U capture. We should note that the average ratios do agree within experimental uncertainty for both cores.

Considering Table XXIII in terms of reaction-rate ratios, we see that the C/E for c^{28}/f^{49} averages about 1.08. This discrepancy has been noted throughout the DEMO Benchmark series of critical experiments [30]. The C/E ratios for ^{238}U fission are quite low, around 0.9. The measurements have not been cell-averaged, but cell averaging would still leave about 5% discrepancy.

The 12% difference in C/E for ^{238}U fission in the radial blanket is not entirely surprising. Because the high energy flux, and hence the ^{238}U fission rate, falls off so rapidly in the blanket, both the measurement and calculation are difficult. The principal difference is in the measurements, but they are the same within the experimental uncertainties.

In Figs. 15-22 we present comparative maps of absolute reaction rates and C/E ratios. A slight bias in absolute reaction rates is possibly due to a change in efficiency of the power monitoring detector (PICO No. 1) when the H240 sector was loaded. If present, this effect would be very small (< 1%).

Considering first the Pu fission map (Fig. 15), we see that within statistical uncertainty, there is very little difference between the normal and the H240 case. This was to be expected from previous results with the fission counter. The comparison holds for the vertical traverse as well as the horizontal. Little difference between cases can be observed in the C/E map presented in Fig. 16. The H240 results tend to be marginally higher than the normal results.

The absolute ^{238}U capture rates are presented in Fig. 17. ^{238}U capture is systematically, if not significantly, lower in the H240 case. This is probably due to the hardening of the low energy spectrum that was observed in the Doppler measurements. In Fig. 18 we observe that the H240 C/E ratios are consistently higher than those for the normal core.

The $^{238}U(n,f)$ map results are found in Figs. 19 and 20. The measured absolute fission rates are mostly within statistics for the two cases. The C/E map shows a generally higher calculated-to-experimental ratio in the high-^{240}Pu case. The results diverge somewhat in the radial blanket, an area of difficulty for both the measurement and the calculation. There is a large statistical uncertainty for the measurement in this region.

Figures 21 and 22 present the ^{235}U fission information. The absolute fission rate was consistently lower in the H240 core. Again, the difference

TABLE XXIII. Comparison of Average Reaction Rate C/Es

Reaction	Region	Reference Core		H240-Zoned Core	
		No. of Points	$\overline{C/E}$ [a]	No. of Points	$\overline{C/E}$ [a]
^{239}Pu(n,f)	Inner Core	18	1.000 ± 0.020	11	1.000 ± 0.017
^{239}Pu(n,f)	Outer Core	25	1.004 ± 0.034	8	1.008 ± 0.028
^{239}Pu(n,f)[b]	Radial Blanket	6	0.997 ± 0.021	3	1.020 ± 0.023
^{235}U(n,f)[b]	Inner Core	42	1.011 ± 0.017	22	1.022 ± 0.015
^{235}U(n,f)[b]	Outer	39	1.001 ± 0.028	16	1.024 ± 0.026
^{235}U(n,f)[b]	Radial Blanket	28	0.988 ± 0.050	11	0.991 ± 0.058
^{238}U(n,γ)	Inner Core	42	1.073 ± 0.019	22	1.095 ± 0.017
^{238}U(n,γ)	Outer Core	39	1.079 ± 0.036	15	1.093 ± 0.037
^{238}U(n,γ)	Radial Blanket	28	1.043 ± 0.048	11	1.048 ± 0.059
^{238}U(n,f)[b]	Inner Core	42	0.874 ± 0.037	22	0.889 ± 0.038
^{238}U(n,f)[b]	Outer Core	39	0.901 ± 0.111	15	0.924 ± 0.061
^{238}U(n,f)[b]	Radial Blanket	28	0.819 ± 0.141	11	0.937 ± 0.127

[a] Normalized such that $\overline{C/E}$ for Pu(n,f) is 1.000 in the inner core. Uncertainties are one standard deviation for C/E.

[b] No cell-averaging factors applied.

Fig. 15. The ^{239}Pu(n,f) Reaction Rates ($\times 10^{-14}$/aton/watt-hour).

H240
REF

117

118

119

120

0.94

121

122   0.99

123

0.95
0.95

124   0.99

125   0.98   0.97   0.95   0.97

126   0.99   0.98

127   0.99 0.98 0.98

128   1.03   1.01   0.97
0.97

129   0.99   1.00 1.00

130   1.00   1.01 1.00   1.01   0.98

131

132   1.02

133   1.00 1.02   1.01

134   1.02   1.00   0.99
0.98

135   1.00   0.98

136   1.02 1.02   0.99

137   1.01 1.03

| | 14 | 15 | 16 | 17 | 18 | 19 | 20 | 21 | 22 | 23 | 24 | 25 | 26 | 27 | 28 | 29 | 30 | 31 | 32 | 33 | 34 | 35 | 36 |

Fig. 16.   The ^{239}Pu(n,f) C/E Map for ZPPR Assembly 4, Phase 2.

Fig. 17. The $^{238}U(n,\gamma)$ Reaction Rates ($\times 10^{-15}$/atom/watt-hour).

Fig. 18. The $^{238}U(n,\gamma)$ C/E Map for ZPPR Assembly 4, Phase 2.

H240
REF

117

118

119

120

121

122

123

124

125

126

127 0.50

128

129

130

131

132

133

134

135

136

137

	0.05
	0.05
	0.07
	0.13
	0.26
	0.26

0.03 0.08

0.06 0.21 0.68 / 0.99 / 0.97

0.18 0.85 1.07 1.18 / 1.30 / 1.32

0.07 0.29 0.41

0.86 / 0.49 0.86 1.31 1.31 1.33

0.20 1.17 1.35 1.45 1.36 1.42 1.43

1.22 1.27 1.34 1.52

0.11 0.18 0.30 1.04 1.26 1.28 1.52 1.56

0.28 0.64 1.22 1.33 1.31 1.31 1.24 1.63

0.06 0.90 1.08 1.14 1.23 1.40 1.28/1.29 1.41 1.68 1.66 / 1.71

1.15 1.55 1.85

1.15 / 1.30 1.52

1.32 1.25 1.59 1.70 1.79 1.72

0.93 1.23/1.14 1.74 1.80 1.79 / 1.80

1.23 1.23 1.53 1.87 1.88 1.75

1.16 1.30 1.81 1.69 / 1.67

0.02 0.04 0.06 0.11 0.93 1.03 1.14 1.04 1.25 1.44 1.57 1.4 1.78 1.69 1.57
0.04 0.06 0.07 0.12 0.23 0.42 0.93 1.01 1.13 1.12 1.35 1.50 1.59 1.67 1.71 1.74 1.80 1.74 1.72 1.56

14 15 16 17 18 19 20 21 22 23 24 25 26 27 28 29 30 31 32 33 34 35 36

Fig. 19. The ^{238}U(n,f) Reaction Rates ($\times 10^{-15}$/atom/watt-hour).
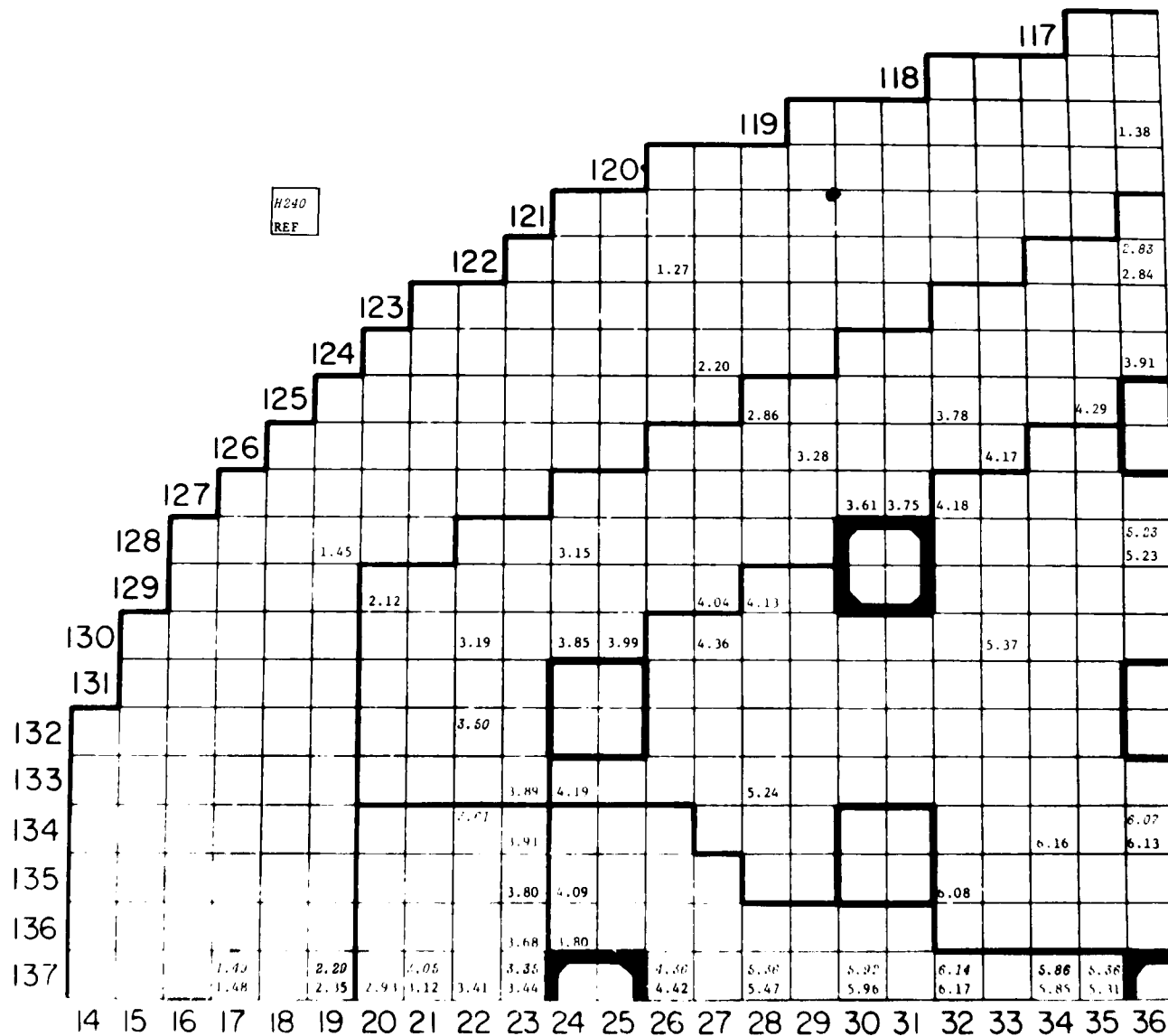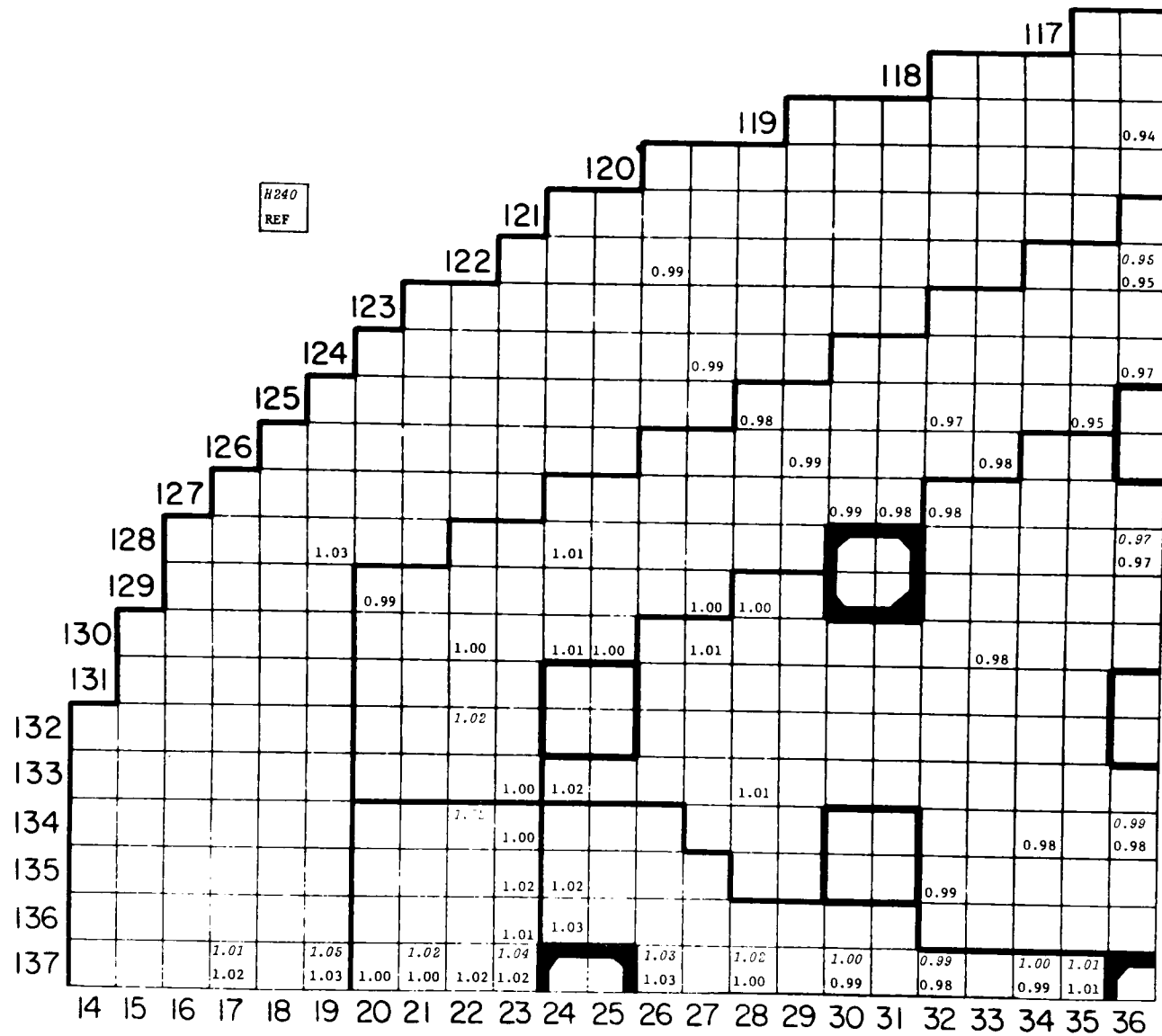
Fig. 20. The ^{238}U(n,f) C/E Map for ZPPR Assembly 4, Phase 2.

Fig. 21.   The $^{235}U(n,f)$ Reaction Rates ($\times 10^{-14}$/atom/watt-hour).

Fig. 22. The ^{235}U(n,f) C/E Map for ZPPR Assembly 4, Phase 2.

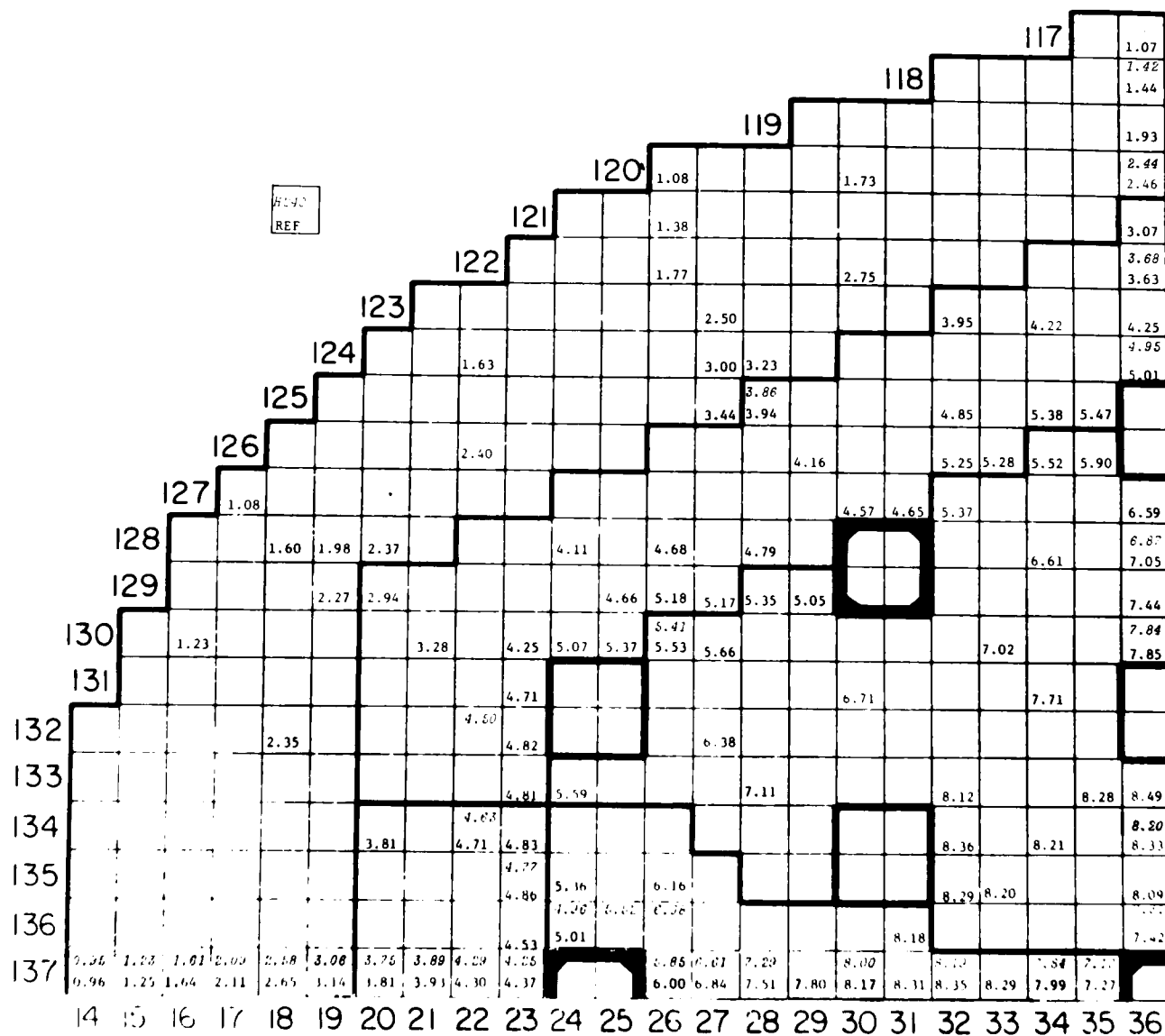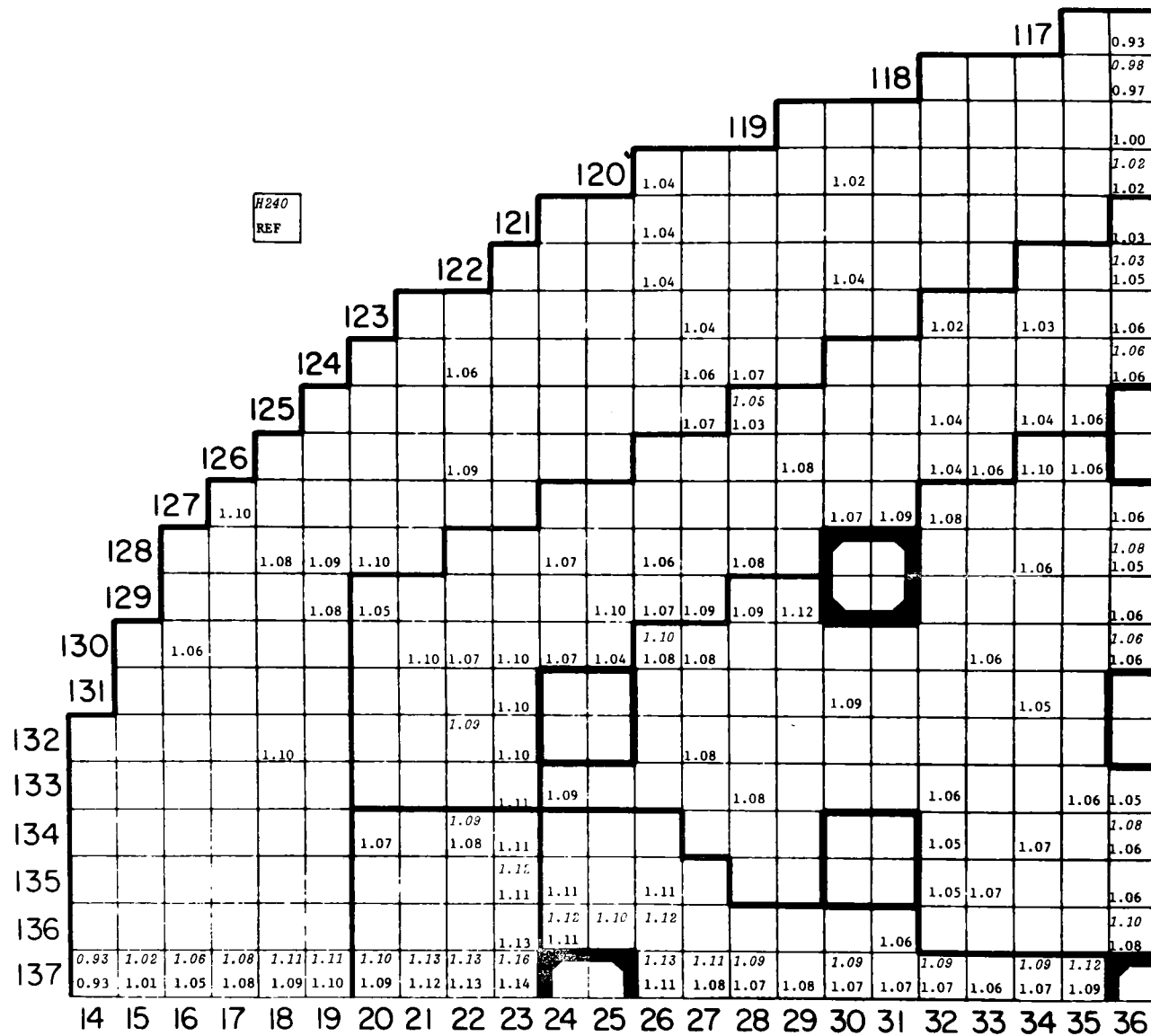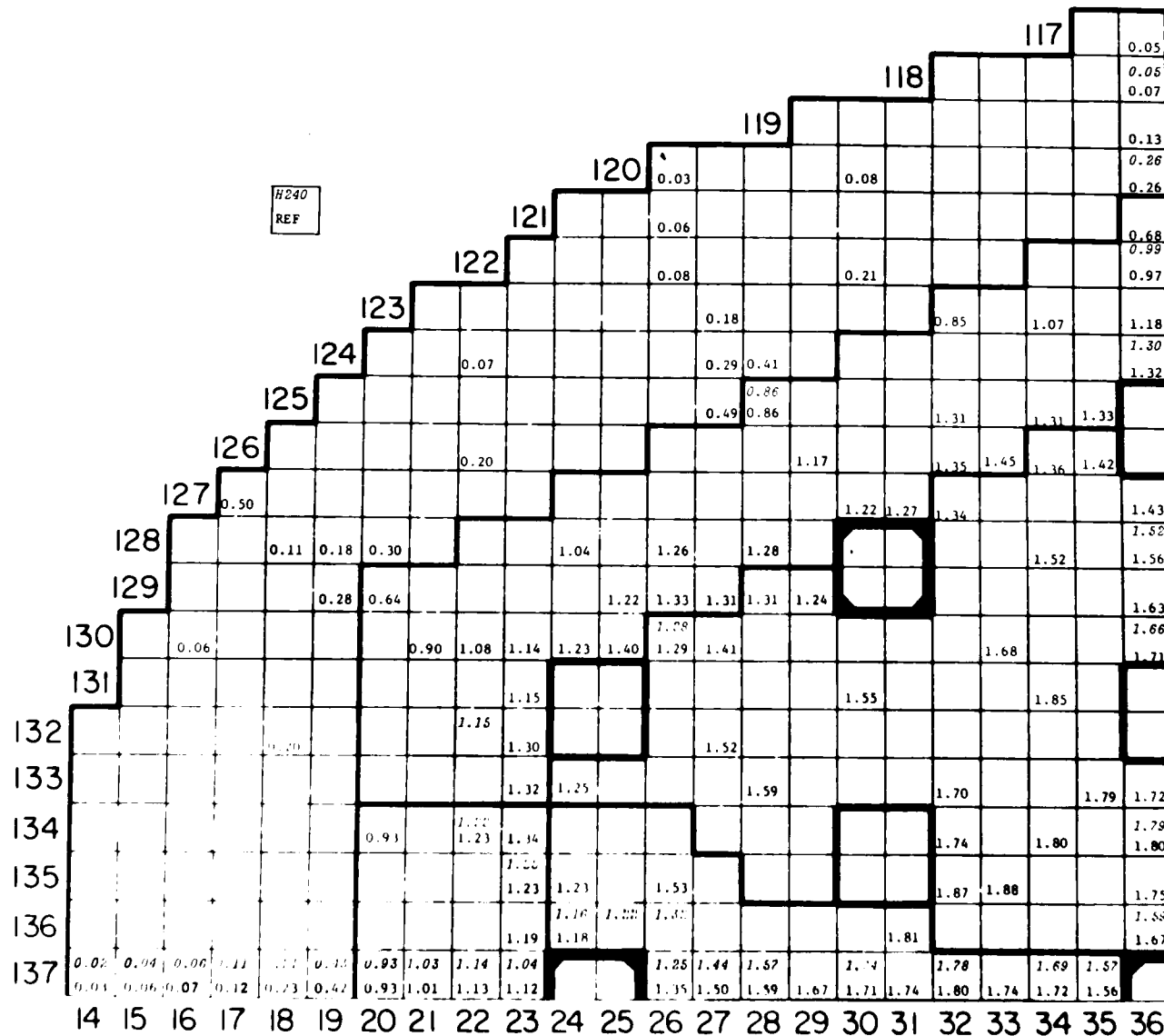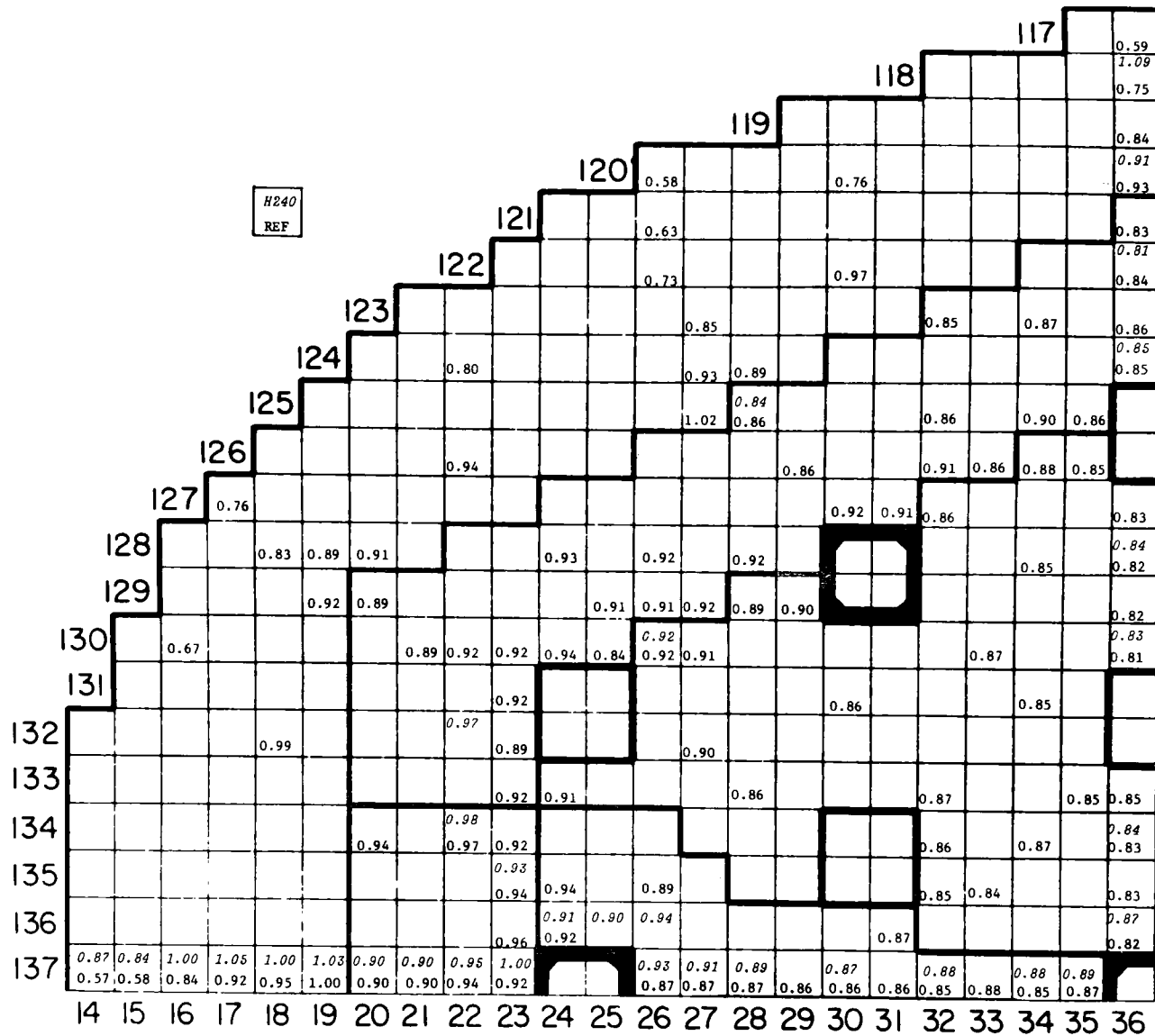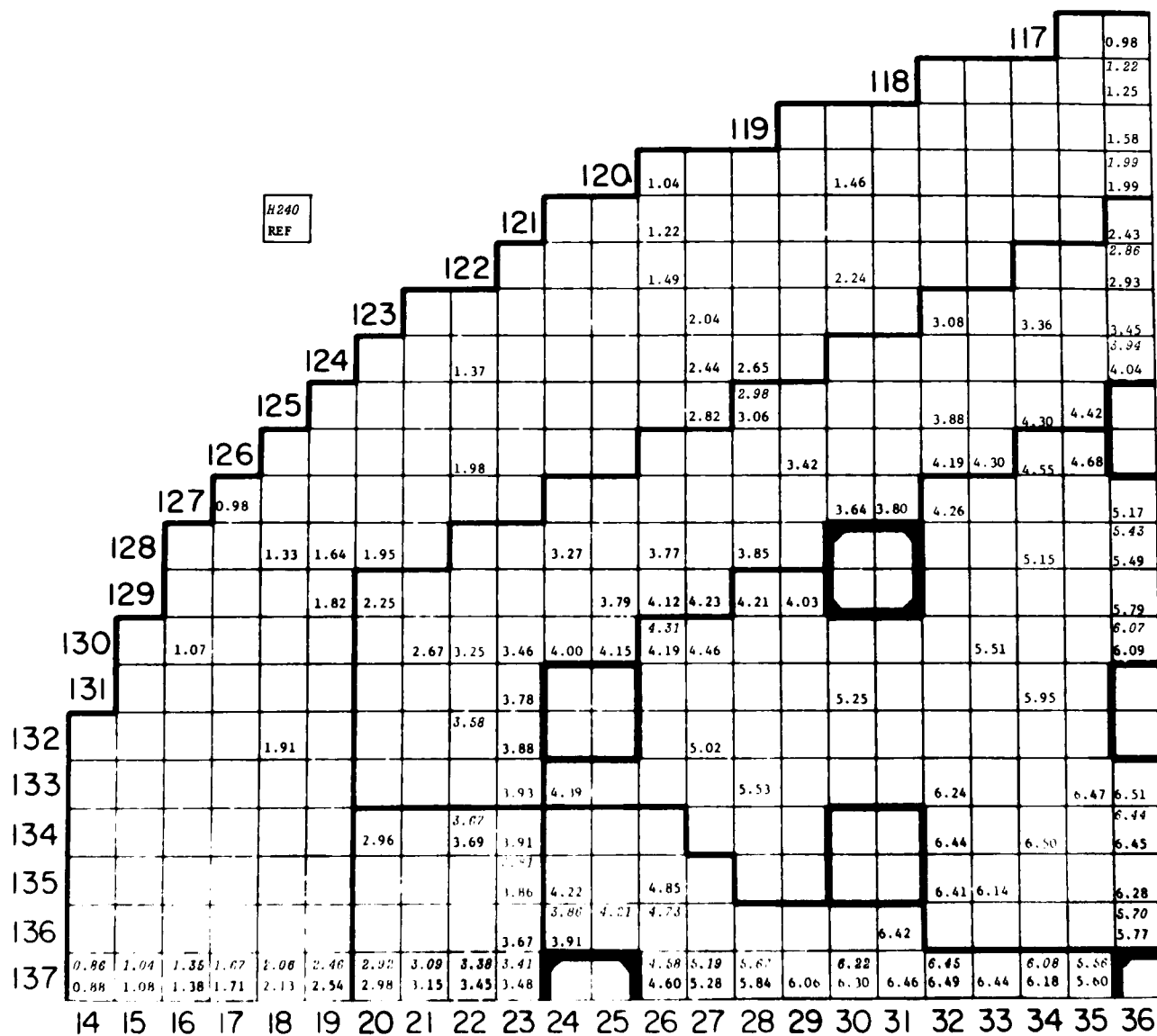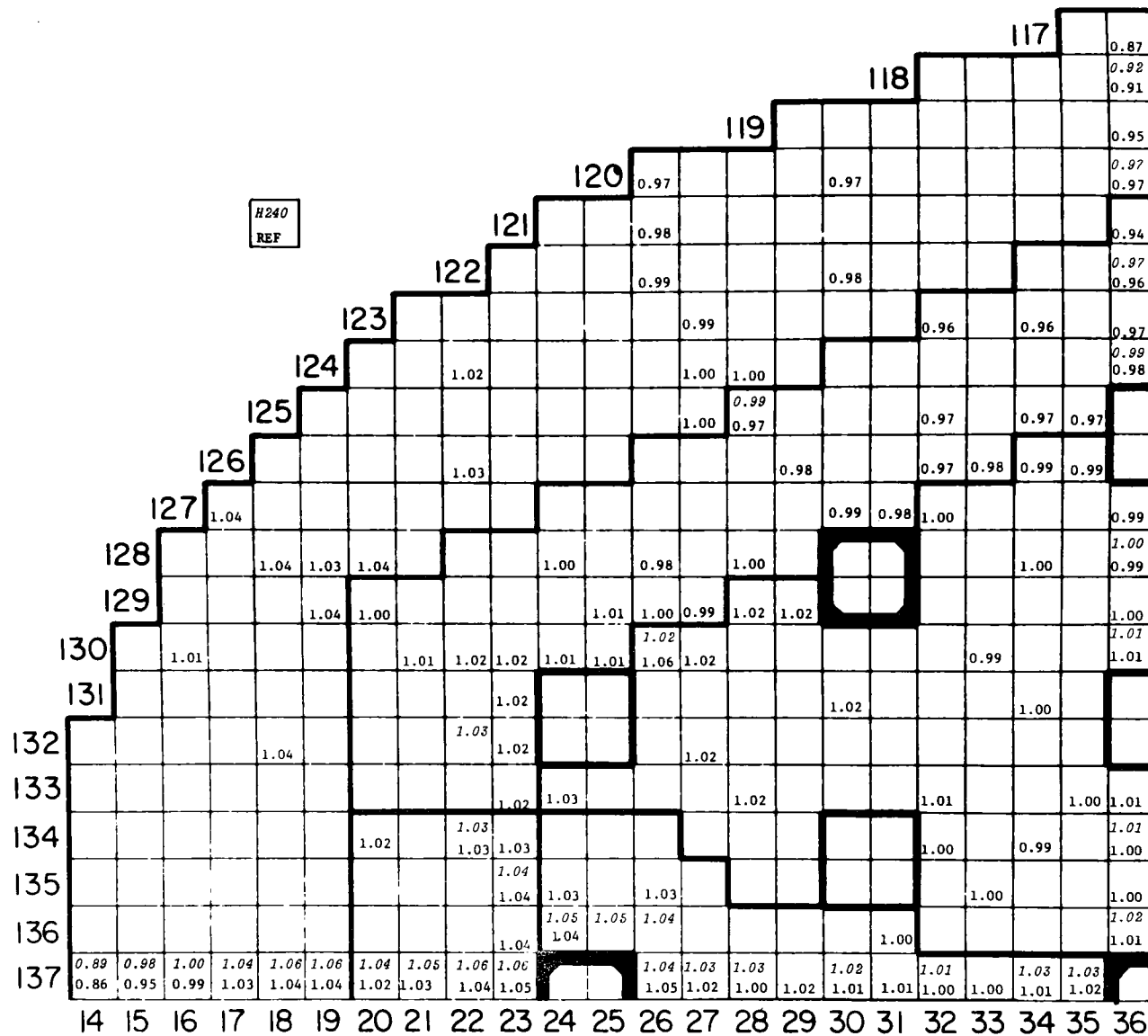was slight and was reflected in higher C/E ratios in the H240 case.

Comparisons of reaction rates measured in the H240 sector and in symmetric positions in the normal ZPPR fuel portion of the core are presented in Tables XXIV – XXVII. For ^{239}Pu fission, ^{235}U fission, and ^{238}U capture, the reaction rates are higher out of the H240 zone. ^{238}U fission is the notable exception, exhibiting higher reaction rates in the H240 zone. This reflects the harder spectrum in the H240 sector. All four types of reactions have generally higher C/E ratios in the H240 zone. By comparing Tables XXIV – XXVII and the absolute reaction rate maps, one can see that the values measured on the right side of the H240-zoned core agree favorably with values measured in the normal core.

VI. SUMMARY

There are two major conclusions to be drawn from the ZPPR assembly 4 high-^{240}Pu studies. The first is that the critical enrichment changes in a significant, yet predictable, manner when the H240 fuel was loaded. The second is that we gathered no evidence to indicate that our ability to calculate the physics parameters in the high-^{240}Pu core differs significantly from that in the normal ZPPR-fueled core.

Two substantial changes resulted from the insertion of the high-^{240}Pu fuel. The first was the 4% reduction in fuel enrichment within the sector. The 10% reduction in the magnitude of the Doppler coefficient was the second major change. Each of these results was expected from previous criticals work with the H240 fuel.

Both the small-sample measurements and the control rod substitution measurement displayed small changes with the installation of the H240 sector. Comparative calculations were able to predict the direction if not the full magnitude of these changes. C/E ratios for the two cases varied by less than 2%.

The sodium-void reactivity measurements are difficult to interpret. On a percentage basis, the reactivity change from the normal to the H240 case was large. In both cases, however, the measured sodium-void reactivity was no more than 11 Inhours. Differences between the support calculations and the experimental results were small in an absolute sense, larger on a percentage basis. The changes should not be attributed to a simple shift in the spectrum. Despite the careful loading of the H240 sector, there are apparent differences in the flux gradients in the outer core which significantly influence the sodium void results. Because of the suspected change in gradients and the small magnitude of the measured reactivity, it is difficult to attach much significance to the comparison between the H240 and normal sodium-void results.

Only minor changes were noted in the reaction rates. Choosing a different normalization would have caused most of the observed changes to disappear. The C/E ratios were slightly higher in the H240 case. Hardening of the spectrum by the H240 fuel did cause a slight increase in the ^{238}U fission rate.

TABLE XXIV. Comparison of ^{239}Pu(n,f) Reaction Rates Measured[a] in the H240 Zone and in Symmetric Positions on the Opposite Side of the Reactor

	H240 Zone			Symmetric Zone	
Matrix Position	10^{-14} Fissions/ Atom/Watt-hour	C/E	Matrix Postion	10^{-14} Fissions/ Atom/Watt-hour	C/E
137-19	2.282	1.051	137-54	2.409	1.017
132-22	3.502	1.022	132-51	3.582	1.005
134-22	3.607	1.025	134-51	3.709	1.001
137-23	3.351	1.040	137-50	3.452	1.012
137-26	4.358	1.033	137-47	4.525	1.005
137-32	6.142	0.991	137-41	6.188	0.980
137-35	5.321	1.006	137-38	5.339	1.010

[a]Uncertainty on measurement about 1%.

TABLE XXV. Comparison of $^{238}U(n,\gamma)$ Reaction Rates Measured[a] in the H240 Zone and in Symmetric Positions on the Opposite Side of the Reactor

	H240 Zone			Symmetric Zone	
Position	10^{-15} Captures/ Atom/Watt-hour	C/E	Matrix Position	10^{-15} Captures/ Atom/Watt-hour	C/E
137–15	1.228	1.02	137–58	1.242	1.03
137–17	2.085	1.08	137–56	2.090	1.09
137–19	3.062	1.11	137–54	3.122	1.11
137–21	3.888	1.13	137–52	3.947	1.11
132–22	4.496	1.09	132–51	4.604	1.07
134–22	4.630	1.09	134–51	4.732	1.07
137–23	4.251	1.16	137–50	4.197	1.13
130–26	5.410	1.10	130–47	5.474	1.07
137–26	5.851	1.13	137–47	5.939	1.09
125–28	3.863	1.05	125–45	3.816	1.06
137–28	7.292	1.09	137–45	7.328	1.09
137–30	7.997	1.09	137–43	8.112	1.08
137–32	8.195	1.09	137–41	8.284	1.08
137–34	7.842	1.09	137–39	7.815	1.10
137–35	7.102	1.12	137–38	7.187	1.11

[a]Uncertainty on measurement about 1%.

TABLE XXVI. Comparison of ^{238}U(n,f) Reaction Rates Measured[a] in the H240 Zone and the Symmetric Positions on the Opposite Side of the Reactor

| | H240 Zone | | | Symmetric Zone | |
Matrix Position	10^{-15} Fissions/ Atom/Watt-hour	C/E	Matrix Position	10^{-15} Fissions/ Atom/Watt-hour	C/E
137-15	0.040	0.84	137-58	0.052	0.66
137-17	0.111	1.05	137-56	0.140	0.84
137-19	0.433	1.03	137-54	0.431	1.01
137-21	1.031	0.90	137-52	1.028	0.88
132-22	1.155	0.97	132-51	1.211	0.93
134-22	1.223	0.95	134-51	1.155	1.03
137-23	1.044	1.00	137-50	1.072	0.96
130-26	1.282	0.92	130-47	1.229	0.96
137-26	1.247	0.93	137-47	1.263	0.93
125-28	0.858	0.84	125-45	0.794	0.93
137-28	1.574	0.89	137-45	1.551	0.89
137-30	1.737	0.87	137-43	1.670	0.88
137-32	1.780	0.88	137-41	1.760	0.86
137-34	1.693	0.88	137-39	1.681	0.87
137-35	1.566	0.89	137-38	1.569	0.87

[a] Not cell averaged. Uncertainty on measurement about 5%.

TABLE XXVII Comparison of ^{235}U(n,f) Reaction Rates Measured[a] in the H240 Zone and in Symmetric Positions on the Opposite Side of the Reactor

| | H240 Zone | | | Symmetric Zone | |
Matrix Position	10^{-14} Fissions/ Atom/Watt-hour	C/E	Matrix Position	10^{-14} Fissions/ Atom/Watt-hour	C/E
137-15	1.039	0.98	137-58	1.096	0.94
137-17	1.672	1.04	137-56	1.761	1.01
137-19	2.465	1.06	137-54	2.545	1.04
137-21	3.088	1.05	137-52	3.192	1.01
132-22	3.379	1.03	132-51	3.649	1.01
134-22	3.672	1.06	134-51	3.745	1.01
137-23	3.414	1.06	137-50	3.463	1.04
130-26	4.314	1.02	130-47	4.388	1.01
137-26	4.585	1.04	137-47	4.665	1.03
125-28	2.985	0.99	125-45	2.924	1.01
137-28	5.669	1.03	137-45	5.834	1.00
137-30	6.217	1.02	137-43	6.388	1.00
137-32	6.451	1.01	137-41	6.480	1.01
137-34	6.080	1.03	137-39	6.147	1.01
137-35	5.557	1.03	137-38	5.572	1.03

[a]Not cell averaged. Uncertainty on measurement about 1%.

An overview of the entire H240 sector experiment suggests that there were no real surprises. There was verification that most of the changes in physics parameters could have been predicted from previous work on the criticals. In general, the support calculations adequately predicted the measured changes.

REFERENCES

1. E.M. Bohn, L.G. LeSage, and J.E. Marshall, "Measurements in ZPR-6 Assembly 7 With the High-240 Plutonium Zone," *Applied Physics Division Annual Report*, July 1, 1970 - June 30, 1971, ANL-7910, p. 102 (1972).

2. A.L. Hess, R.W. Goin, and S.G. Carpenter, "Single Rod Experiments in Phase 1 of ZPPR Assembly 4," ANL-RDP-25, pp. 6.5 - 6.11 (Feb. 1974).

3. R.E. Kaiser, "Control-Rod Group Worth Measurements," ANL-RDP-25, pp. 6.11 - 6.13 (Feb. 1974).

4. A.L. Hess and D.N. Olsen, "Assembly 4, Phase 2, High-^{240}Pu Zoned Reference Core," ANL-RDP-28, pp. 6.6 - 6.11 (May 1974).

5. R.E. Kaiser, "Approach to Critical, Phase 2, IC-BOC Configuration," ANL-RDP-26, p. 6.1 (March 1974).

6. C.L. Beck, "ZPPR Assembly 4 Analytical Support," ANL-RDP-28, pp. 6.17 - 6.19 (May 1974).

7. H.F. McFarlane, "The Critical Configurations for the Parked Rod and the IC-BOC Experiments in ZPPR Assembly 4," ANL-RDP-39, pp. 6.26 - 6.27 (April 1975).

8. R.E. Kaiser, Argonne National Laboratory, unpublished information (1971).

9. E.M. Bohn, L.G. LeSage, and J.E. Marshall, "Measurements in ZPR-6 Assembly 7 With the High-240 Plutonium Zone," *Applied Physics Division Annual Report*, July 1, 1970 - June 30, 1971, ANL-7910, pp. 102-112 (1972).

10. W.M. Stacey, Jr. et al., "A New Space-Dependent Fast-Neutron Multigroup Cross-Section Preparation Capability," *Trans. Am. Nucl. Soc.*, 15, 292 (1972).

11. D.E. Neal, et al., *The ARC System One-Dimensional Diffusion Theory Capability, DARC1D*, ANL-7715 (1971).

12. T.A. Daly, et al., *The ARC System Two-Dimensional Adjunct Calculations*, ANL-7720 (1972).

13. R.W. Hardie and W.W. Little, Jr., *PERT-V, A Two-Dimensional Perturbation Code for Fast Reactor Analysis*, Battelle Memorial Institute Report, BNWL-1162 (1969).

14. G.L. Grasseschi, Argonne National Laboratory, private communication.

15. R.W. Goin, C.L. Beck, D.N. Olsen, and H.F. McFarlane, "Small Perturbation Sample Traverses in ZPPR Assembly 4, Phase 2, IC-BOC," ANL-RDP-30, pp. 6.5 - 6.6 (July 1974).

16. C.L. Beck, R.W. Goin, D.N. Olsen, and H.F. McFarlane, "Small-Perturbation Sample Traverses in ZPPR Assembly 4, Phase 2, the H240 Zone, and EC-MOC," ANL-RDP-31, pp. 6.6 - 6.10 (August 1974).

17. R.W. Goin, M.J. Lineberry, H.F. McFarlane, and R.E. Kaiser, "Reactivity Worths for Small Perturbation Samples in ZPPR Assembly 3, Phase 1B and 2," ANL-RDP-15, pp. 8.1 - 8.7 (March 1973).

18. P.J. Collins and R.G. Palmer, "Calculated Size Effects for Reactivity Samples in ZPPR," *Applied Physics Division Annual Report,* July 1, 1970 to June 30, 1971, ANL-7910, p. 247 (1972).

19. R.E. Kaiser, "Natural UO_2 Doppler Measurements in the ZPPR Assembly 4 Phase 2, High-^{240}Pu Zone," ANL-RDP-27, p. 6.14 (April 1974).

20. R.E. Kaiser, "Doppler Measurements," ANL-RDP-31, pp. 6.1 - 6.3 (August 1974).

21. R.E. Kaiser, J.M. Gasidlo, and W.G. Davey, "Reactivity Doppler Measurements in ZPPR Assembly 2," *Applied Physics Division Annual Report,* July 1, 1970 to June 30, 1971, ANL-7910, pp. 265-270 (1972).

22. J.M. Gasidlo, R.E. Kaiser, D.P. Pruett, and J.C. Young, "Effectiveness of the Dual Heater Temperature Control System in the ZPPR Doppler Reactivity Mechanism," *Applied Physics Division Annual Report,* July 1, 1970 to June 30, 1971, ANL-7910, pp. 414-417 (1972).

23. R.E. Kaiser, J.M. Gasidlo, and W.G. Davey, "Reactivity Doppler Measurements in ZPPR Assembly 2," *Applied Physics Division Annual Report,* July 1, 1970 to June 30, 1971, ANL-7910, pp. 265-270 (1972).

24. D.N. Olsen, "Worth of Control Rod Substitution in the High-^{240}Pu Zoned Configuration of ZPPR Assembly 4, Phase 2," ANL-RDP-28, pp. 6.12 - 6.13 (May 1974).

25. J.M. Gasidlo, S.G. Carpenter, G.R. Thayer, and R.W. Goin, "Measured Worths of Control-Rod Groups in the IC-BOC Configuration of ZPPR-4, Phase 2," ANL-RDP-36, pp. 6.2 - 6.4 (January 1975).

26. R.E. Kaiser, "Evaluation of Detector Efficiency and Source Worth Corrections for Subcritical Reactivity Measurements in a Fast Critical Assembly," *Nuclear Technology, 25,* pp. 138-149 (January 1975).

27. A.M. Broomfield, P.J. Collins, M.D. Carter, J. Marshall, A. Sugawara, Y. Sekiguchi, T. Konishi, "The Mozart Control Rod Experiments and Their Interpretation," *Proc. of International Symposium on Physics of Fast Reactors,* Tokyo, October 16-19, 1973, pp. 312-334.

28. G.G. Simons and T.S. Huntsman, "ZPPR Assembly 4 Gamma Ray Heating," ANL-RDP-36, pp. 6.4 - 6.5 (January 1975).

29. D.W. Maddison and J.M. Gasidlo, "Foil Measurements in ZPPR Assembly 4, Phase 2," ANL-RDP-33, pp. 6.5 - 6.10 (October 1974).

30. W.G. Davey, "The Demonstration Reactor Benchmark Program," *Proc. of Conference on New Developments in Reactor Physics and Shielding,* Sept. 12-15, 1972, Kiamesha Lake, NY, Conf-720901, pp. 789-808.

Distribution of ANL-76-112

Internal:

J. A. Kyger
A. Amorosi
R. Avery
L. Burris
S. A. Davis
B. R. T. Frost
D. C. Rardin
R. G. Staker
R. J. Teunis
C. E. Till
R. S. Zeno
P. Amundson
C. L. Beck
S. Carpenter
P. Collins
L. Emmons
R. Forrester
J. Gasidlo
R. Goin
C. Grasseschi
R. Kaiser
J. Larson
M. Lineberry
P. McCarthy
H. McFarlane (10)
D. Maddison

D. Olsen
C. Payne
E. Puckett
P. Schaffer
G. Simons
F. Thalgott
G. Thayer
W. Windmiller
D. Rock
W. Barthold
E. Gelbard
H. Henryson
H. Hummel
P. Kier
R. Lewis
J. Snelgrove
W. Stacey
W. Sturm
B. Toppel
A. Travelli
R. Armani
E. Bennett
R. Beyerlein
S. Bhattacharyya
E. Bohn

M. Bretscher
R. Bucher
R. Cornella
L. Dates
K. Freese
L. LeSage
F. LeVert
G. Lowe
F. Martens
R. McKnight
J. Morman
N. O'Fallon
R. Pond
K. Porges
W. Robinson
G. Rusch
R. Schaefer
R. Scharping
A. B. Smith
D. M. Smith
D. Wade
T. Yule
J. Cassady (5)
ANL Contract File
ANL Libraries (5)
TIS Files (6)

External:

ERDA-TIC, for distribution per UC-79d (233)
Manager, Chicago Operations Office
Chief, Chicago Patent Group
Director, Reactor Programs Div., ERDA-CH
Director, ERDA-RDD (2)
Director, CH-INEL
President, Argonne Universities Association
Applied Physics Division Review Committee:
  R. M. Brugger, Univ. of Missouri, Columbia
  Paul Greebler, General Electric Co., Sunnyvale
  R. L. Hellens, Combustion Engineering, Inc.
  J. M. Hendrie, Brookhaven National Laboratory
  J. S. King, Univ. of Michigan
  W. B. Loewenstein, Electric Power Research Institute